Miguel Alexandre Martins Franco

Licenciado em Engenharia de Micro e Nanotecnologias

Resistance Switching Memory Devices based on Zinc Oxide Nanoparticles on Paper Substrates

Dissertação para Obtenção do Grau de Mestre em
Engenharia de Micro e Nanotecnologias

Orientador:	Doutor Luís Miguel Nunes Pereira, Professor Auxiliar, Faculdade de Ciências e Tecnologia da Universidade Nova de Lisboa
Co-orientadora:	Doutura Asal Kiazadeh Professora Auxiliar, Faculdade de Ciências e Tecnologia da Universidade Nova de Lisboa

Júri

Presidente:	Doutor Rodrigo Ferrão de Paiva Martins, Professor Catedrático, Faculdade de Ciências e Tecnologia da Universidade Nova de Lisboa
Arguente:	Doutora Joana Maria Dória Vaz Pinto, Professora Auxiliar, Faculdade de Ciências e Tecnologia da Universidade Nova de Lisboa
Vogal:	Doutor Luís Miguel Nunes Pereira, Professor Auxiliar, Faculdade de Ciências e Tecnologia da Universidade Nova de Lisboa

FACULDADE DE CIÊNCIAS E TECNOLOGIA
UNIVERSIDADE NOVA DE LISBOA

Setembro 2016

Resistance Switching Memory Devices based on Zinc Oxide Nanoparticles on Paper Substrates

© Miguel Alexandre Martins Franco

Faculdade de Ciências e Tecnologia

Universidade Nova de Lisboa

ACKNOWLEDGMENTS

I want to thank the people that doesn't respect me, constantly trying to destabilize me and even worse, thinking that I am an unconscious person who dedicates and help them. Sorry to say, but I will give bad news to these people. Despite of being a dedicate and helpful person I'm not blind and I hate when people try to foul me. Their attempts to cause my failure are just a force and a motivation to follow my dreams. Probably these lines that I have dedicated in this work won't be read for who wanted to possess my feelings and make my life a beautiful lie. I won't provide the names of these people because I respect these people despite the damage taken. They are now ghosts haunting in my head, screams from the past that I remember today.

I have dreams. I fight for them. My imperfections and failures are my motivation to be a better person. I want to be improve to reach perfection. When I reach the utopia it will be my doom. Perfection means the end of a journey, the end of a life. With perfection the motivation banishes along the air that I need to live.

I want to live in a better world. I want to ensure the next generations have a green planet to live, preserve and respect. I want to live in a planet where everyone is conscious and aware the problems and challenges. This is my wishes, this is my thoughts when I throw a coin into the bottom of a well, when I'm looking to a shooting star, aware the situation won't be changed by wishing and wait for other to do and fight. I became frustrated and disappointed to watch the situation of this condemned civilization. People only worries about his commodity, ignoring the real problems that could ruin the prosperity of our society. People are enslaved with gadgets, like kittens playing with a rope while some influent people easily manipulates with two objectives: power and money. I start to became worried because our society are numb and ignorant. I see a Europe full of good ideals being corrupted by lobbyists, causing the inevitable destruction process of a utopic European Union of a disunited members and lost voices.

I'm here trying to make the world a better place to live. This is the reason I've entered to Micro and Nanotechnology Engineering at FCT-UNL. I wanted to expand my knowledge, to learn the tools needed to the search of knowledge. Five years have passed and I'm one step to be graduated. It was a privilege to be able to integrate in a creative and prestigious team like CENIMAT|i3N and CEMOP, for me a worldwide pioneer in paper electronics. A restless demand in order to overcome barriers and open new horizons in scientific knowledge are a constant in these centres, developing innovative, challenging and current work applied in different areas. Therefore, first of all I would like to thank Professor Rodrigo Martins and Professor Elvira Fortunato for the access to these installations and technology. Their multidisciplinary knowledge, competence and commitment allow the excellent conditions of work here in CENIMAT|i3N and CEMOP. In addition, I would like to thank for the fact of being able to open this unique and outstanding integrated masters in Portugal.

Secondly, I would like to express my sincere gratitude to my supervisor, Professor Luís Pereira for accepting and give me the chance to join and work in his research group. I cannot thank you enough for all support, encouragement, valuable suggestions, availability and the spirit of research, your inspiring enthusiasm. I am also grateful for all the support given by his extraordinary group of researchers including Tiago Carvalho, Paul Grey, Inês Cunha, Diana Gaspar, Raquel Barras and Pedro Freitas. For all the advices, knowledge, the inspiring long hours of hard-working spent in the. Thank you for always finding time to discuss the things that you guys well know. Once again, thank you Tiago for your relevant and innovative suggestions and for always find time to help in every possible way. Essentially, thanks to all of you and especially to Professor Luís for installing this team and work spirit.

In order to not forget anyone, I would like to express my gratitude to the rest of these both institutes for the support and the relevant suggestions.

Also, I am a grateful to my colleagues and course mates of Micro and Nanotechnology and Materials Science as well. Thanks for the support with the tasks from those different areas during this degree.

Also I want to thank you my family to make the biggest motivation.

And thank you Bia (I’m not forgetting you) for being my right arm during this journey and making read and correct my nonsense.

ABSTRACT

This work reports the development of resistive random access memory (RRAM) on paper using printed Zinc Oxide (ZnO) nanoparticles (NPs) as active layer. RRAM is a novel technology having attracted increasing attention due to their high-speed operation, high-density storage, and low voltage. Most important, due to its characteristics it could replace flash technology which suffers from low endurance, low write speed, and high voltages required for the write operations.

Screen printing was chosen because of its versatility in terms of ink viscosity, which is compatible with inks that require low annealing temperatures. The architecture adopted consists in a mixture of ZnO NPs and ethyl cellulose (EC), used as binder, between electron beam evaporated platinum bottom electrode and screen-printed carbon or silver top electrode.

The resistive memory device can be programed in bipolar for at most 20 cycles. The retention time of the bipolar switching for both on/off states is reached up to 10 Ks. The operating voltages of SET and RESET is high ~ 20 V and - 10 V respectively. A transition between bipolar switching to unipolar is observed. It is suggested that an instable bipolar resistive switching is due to growth of filaments during cycles. The required voltages for on/off states fluctuate in the range of ~ 5 V which is a strong evidence of non-consistent bipolar resistive switching.

Keywords: Zinc oxide, ethyl cellulose, paper electronics, resistive random access memory, printed electronics, screen-printing

RESUMO

Este trabalho reporta o desenvolvimento das memórias resistivas em substrato de papel usando nanopartículas (NPs) de óxido de zinco (ZnO) e de etilcelulose (EC), como camada ativa. As memórias de acesso aleatório resistivas (RRAM) são uma tecnologia recente que tem atraído crescente atenção devido á rápida velocidade de operação, alta densidade de armazenamento e baixa temsão de funcionamento. Devido ás suas características poderão substituir a memoria flash que tem como limitações a baixa endurance, baixa velocidade de escrita e altas voltagens para escrever.

A técnica de *screen printing* foi escolhida devido a sua versatilidade em termos da viscosidade da tinta, que torna compatível a criação de tintas que requerem baixa temperatura de recozimento. A arquitetura adotada consiste numa mistura de nanopartículas de óxido de zinco envolvidas em etilcelulose entre contato inferior de platina depositado por evaporação por canhão de eletrões e contato de topo de carbono ou de prata impresso por *screen printing*.

As memorias resistivas podem ser programadas no modo bipolar até 20 ciclos. O tempo de retenção atingido após transição bipolar para ambos os estados *on* e *off* foi de 10 000 segundos. A tensão de operação de *SET* and *RESET* é elevado ~20 V e -10 V respetivamente. A transição entre bipolar e unipolar também é observado. É sugerido que a instabilidade na transição bipolar é devida ao crescimento de filamentos durante o ciclo. A diferença entre valores de tensão dos estados on e off é aproximadamente 5V, que é uma forte evidencia de transição bipolar não consistente.

Palavras-chave: óxido de zinco, etilcelulose, eletrónica em papel, memória de acesso aleatório resistiva, eletrónica impressa, *screen-printing*

LIST OF ABBREVIATIONS

a.u.	Arbitrary units
ATR-FTIR	Attenuated total reflectance - Fourier transform infrared spectroscopy
CEMOP	Centro de Excelência de Optoelectrónica e Microeletrónica de Processos
CAFM	Conductive Atomic Force Microscopy
CENIMAT|i3N	Centro de Investigação de Materiais|Instituto de Nanoestruturas, Nanomodelação e Nanofabricação
CNT	Carbon nanotubes
DI	Deionized
DRAM	Dynamic random access memory
EC	Ethyl cellulose
FeRAM	Ferroelectric random access memory
FTIR	Fourier transform infrared spectroscopy
HRS	High resistance state
LRS	Low resistance state
MIM	Metal-insulator-metal
MRAM	Magnetoresistive random access memory
NVM	Non-volatile memory
RS	Resistive switching
SEM	Scanning electron microscope
SCLC	Space-charge-limited current
SRAM	Static random access memory
UV	Ultraviolet
WORM	Write once read many
wt	Weight total

LIST OF SYMBOLS

d	Film thickness
E	Electrical field
$E_C - E_F$	Activation energy
J	Current density
N_C	Effective density of states
q	Number of electrons
R_{ON}	ON state Resistance
R_{OFF}	OFF state Resistance
V	Voltage
V_{SET}	Set Voltage
V_{RESET}	Reset Voltage
ε_i	Absolute permittivity
σ	Electrical conductivity
μ	Mobility of charge carriers

TABLE OF CONTENTS

ACKNOWLEDGMENTS ..... **I**
ABSTRACT ..... **III**
RESUMO ..... **V**
LIST OF ABBREVIATIONS ..... **VII**
LIST OF SYMBOLS ..... **VII**
TABLE OF CONTENTS ..... **IX**
LIST OF FIGURES ..... **XI**
LIST OF TABLES ..... **XIII**
MOTIVATION ..... **XV**
OBJECTIVES ..... **XV**
1 INTRODUCTION **1**

1.1 Paper as substrate **1**
1.2 Memories: from its most basic definition to RRAM **2**
1.3 Screen Printing technique **3**
1.4 Ink formulation for RRAM fabrication **4**

2 MATERIALS AND METHODS: FABRICATION, OPTIMIZATION AND CHARACTERIZATION OF ZNO RRAM DEVICES **7**

2.1 ZnO ink formulation materials and reagents **7**
2.2 ZnO:EC RRAM by screen-printing **7**
2.3 ZnO RRAM using printing pen **8**
2.4 Characterization techniques **8**

3 RESULTS AND DISCUSSION **9**

3.1 Study of memory effect when using only ZnO NPs as active layer **9**
3.2 Study the memory effect of EC as active layer **11**
3.3 Study the memory effect when using 10% ZnO with 5 % EC as active layer **12**
3.4 Study the memory effect when using 40% ZnO with 5 % EC as active layer **14**

3.4.1 UV irradiation influence on the active layer 15

3.5 Study the influence of active layer (ZnO:EC) thickness **17**

3.5.1 Comparison of electrical performance for different active layer thickness 18
3.5.2 Two printing steps of 40% ZnO:5% EC with silver top contact (40ZnO2Ag) 19
3.5.3 Two printing steps of 40% ZnO:5% EC with silver top contact (40ZnO2Ag) 21

3.6 Three printing steps of 40% ZnO:5% EC with carbon top contact (40ZnO3) **22**

3.6.1 Endurance cycles 23
3.6.2 Retention time 25

3.7 Study of the switching mechanism mode **26**

4 CONCLUSIONS AND FUTURE PERSPECTIVES **31**

4.1 Final conclusions **31**

4.2 Future perspectives 32
5 BIBLIOGRAPHY 33
6 ANNEX 37

LIST OF FIGURES

Figure 1.1 a) Application of a zinc oxide nanorods in textile substrate targeting the development of a diode [6] **b)** Zinc Oxide based memory on stainless steel substrate [7]..... 1
Figure 1.2 - a) Typical I-V curve of a unipolar **b)** and bipolar resistive memory, (adapted from [19]) 3
Figure 1.3 - Schematic representation of the custom-made screen-printing present in CENIMAT|i3N[39]..... 4
Figure 2.1 Schematic representation of the architecture adopted in this work and their conections to the Agilent B1500 Semiconductor parameter analyzer..... 8
Figure 3.1 - Image of the surface of drawn ZnO lines with different number of passages between screen-printed carbon top contacts and E-beam platinum bottom contact on paper substrates..... 10
Figure 3.2 - I-V curves of ZnO between carbon top contact and platinum bottom contact on paper substrate for: **a)** one writing step **b)** three writing steps..... 10
Figure 3.3 - First IV sweep realized during electrical characterization, showing a device in LRS..... 11
Figure 3.4 - a) Endurance cycles performed of EC between carbon top and bottom contact on paper substrate **b)** Rreading tests for 100 s at 500 mV after the SET and RESET the device..... 12
Figure 3.5 - Image of the surface with screen-printed 10% ZnO : 5% EC layer with carbon top contacts on paper substrates..... 12
Figure 3.6 - First I-V sweep realized during electrical characterization, showing a virgin device..... 13
Figure 3.7 - a) First cycle performed on 10 % Zno : 5 % EC with carbon top contact and platinum bottom contact (10ZnO) **b)** Read test for 100 s at 500 mV after the first SET and RESET the device in a)..... 13
Figure 3.8 - Second cycle performed on 10 % Zno : 5 % EC with carbon top contact and platinum bottom contact (10ZnO)..... 14
Figure 3.9 - ATR-FTIR spectra of the ZnO NPs:EC ink after being screen-printed on a glass substrate and submitted or not UV irradiation for 15 min..... 15
Figure 3.10 - Endurance cycles performed on 40 % Zno : 5 % EC with carbon top contact and platinum bottom contact on paper substrate without UV irradiation..... 16
Figure 3.11 - a) average level of resistence at HSR and LSR after the SET and RESET the device in 3.10, comparing to a device that was made UV irradiation after printing the active layer **b)** Reading retention for 1 500 s at 500 mV after SET and RESET the device..... 16
Figure 3.12 - SEM images of device cross sections with 800x of magnification and the ZnO:EC thickness over the distance graphic: **a)** with 1 printing step **b)** with 2 printing steps **c)** with 3 printing steps **d)** with 3 printing steps on another local..... 17
Figure 3.13 - a) 2nd cycle of 40ZnO1C, 40ZnO2C and 40ZnO3C; **b)** HRS current over the cycles for two printing steps and three printing steps of ZnO:EC layer..... 18
Figure 3.14 - Image of the surface with screen-printed 40% ZnO : 5% EC layer and also silver and carbon top contacts on paper substrates..... 19
Figure 3.15 - a) Endurance cycles performed on 40 % Zno : 5 % EC with carbon top contact and platinum bottom contact on paper substrate **b)** Switching probability over voltage **c)**average LRS and HSR current after the SET and RESET the device in a) for 18 cycles..... 20
Figure 3.16 - Retention test for 2500 s at 500 mV..... 20
Figure 3.17 - SET process in 17th and 18th cycle, evidencing the device failure..... 21
Figure 3.18 - a) Endurance cycles performed on 40 % Zno : 5 % EC with silver top contact and platinum bottom contact on paper substrate **b)** retention tests for 10 s at 500 mV after the SET and RESET the device in a)..... 22
Figure 3.19 - Image of the surface of three printing steps of screen-printed 40% ZnO:5% EC between screen-printed carbon top contacts and E-beam platinum bottom contact on paper substrates..... 22
Figure 3.20 - Number of cycles achieved on each contact and also the estimated ZnO:EC layer thickness location in 3.12 c) in blue and 3.12 d) in black..... 23
Figure 3.21 - Inicial IV sweep performed in this device..... 23

Figure 3.22 - a) Endurance cycles performed on 40 % Zno : 5 % EC with carbon top contact and platinum bottom contact on paper substrate; **b)** Switching probability over voltage **c)** average level of resistence at HSR and LSR after the SET and RESET the device in a) 25
Figure 3.23 - Retention test for 10 000 s at 500 mV after SET and RESET the device..... 26
Figure 3.24 – a) Unipolar switching of three printing steps of screen-printed 40% ZnO:5% EC between screen-printed carbon top contacts and E-beam platinum bottom contact on paper substrates **b)** current in LRS and HSR after SET and RESET respectively. 27
Figure 3.25 - Log J vs log V on a device with a top electrode area of 4 mm^2 on a) 5^{th} SET c) 2^{nd} set. 27
Figure 3.26 – Explanation of the filament mechanis in bipolar and unipolar resistance change 29

LIST OF TABLES

Table 1.1-Key parameters of the reported RRAM i.e. the substrate, the active layer, the position technique, te anealing temperature, the electrodes and the endurance..... 3
Table 2.1 - Inks composition developed in this work and its quantity 7
Table 3.1 – All fabricated devices characteristics and their nomenclature..... 9
Table 3.2 - Device characteristics using 40% ZnO ink 14

MOTIVATION

Presently, in a society of consume ruled by capitalism, the economic growth is based on increasing the products sales. With an exponential increase of global population, more products will be manufactured to satisfy the increasing demand. With this model, two consequences will happen: the materials shortage and increasing the waste. In case of consumer electronic, particularly portable electronics, such as smart phones, tablets, personal computers, televisions have helped sustain the economic growth in a majority of the world. However, rapid technological advances have led to a significant decrease in the lifetime of consumer electronics and also rapid consumption of non-renewable natural resources [1]. In 2006, the world's production of E-waste was estimated at 20–50 million tonnes per year (UNEP, 2006), representing 1–3% of the global municipal waste production of 1636 million tonnes per year (OECD, 2008). Cobbing (2008) calculated that computers, mobile telephones and television sets would contribute 5.5 million tonnes to the E-waste stream in 2010, rising to 9.8 million tonnes in 2015. In developed countries, E-waste may constitute some 8% by volume of municipal waste [2].

On average, cell phones are used for 18 months and computers are used for 3 years before being replaced [3]. In fact, in 2007, it was estimated that over 426,000 cell phones (most of them were still functional) and 112,000 computers were discarded every day in the US, totalling 3.2 million tons of electronic waste generated per year [4]. With the past years the emerging countries which represent at least 1/3 of global population started to be led by consuming, the number of devices manufactured increased exponentially. In the second quarter of 2016, 343 000 000 smartphones were produced worldwide. Inevitably, we are reaching a limit to our resources and also to reach the economy growth based on savage consumes. This scenario can be even worst considering the new concept of internet of things (IoT) with more and more devices getting connected (35 billion expected already in 2019). So it is imperative to adopt a sustainable policy for the development of new electronic goods, that could protect the environment and provide a sustainable growth.

The use of biodegradable materials in electronics can reduce the accumulation of persistent solid waste, thereby benefiting our living environment. Moreover, the fabrication of many chips in portable electronic devices involves the consumption of precious and scare materials. In a typical semiconductor electronic chip, the active region comprises the top thin layer and is only a small portion of the chip, whereas the bottom substrate that holds the chip consists of more than 99% of the semiconductor materials. In order to solve or minimize this problem, ‘‘Green’’ materials are an emerging concept within the carbon-based class, aimed at achieving far more ambitious goals, e.g. integration of electronics into living tissue with the aim of achieving biochemical monitoring, diagnostic, or even drug delivery tasks or generating human and environmentally benign technologies [5]. ‘‘Green’’ materials and technologies are carving avenues towards achieving the ambitious goal of sustainability in the field of electronics, by identifying highly abundant and low cost organic precursors, with economically feasible-high throughput synthetic routes that avoid the usage of toxic solvents for the fabrication of electronic grade materials and do not generate toxic waste requiring expensive handling and disposal. In addition, the synthesized electronic grade materials should ensure low cost processing routes in practical devices (ideally either at room temperature from benign solvents or at low sublimation temperatures), and render electronics that feature biodegradability in mild degradation conditions at the end of their life cycle and/or electronics that are suitable for performing complex biological functions (e.g. transduction, sensing, recognition, event triggering, etc.) as a tool for interfacing electronics with various forms of life [5].

Focusing the topic of “green” electronics, this work aims to develop resistive random accesses memories (RRAM), which is a promising technology that could solve the limitations flash memory. To assure environmental friendship and sustainability the paper is selected as substrate, which is a natural, renewable, low-cost and fast fabrication substrate. This work will be make in a high reputation institution CENIMAT|i3N, world pioneer in paper electronics. It will be using as possible low cost techniques and environmental friendly precursors to achieve the objective.

OBJECTIVES

The main purpose of this dissertation is to design, fabricate and characterize RRAM memories, combining cellulose with Zinc Oxide (ZnO) nanoparticles (NPs). The focus will be the development of RRAM on paper substrate, where the ZnO NPs mixed with cellulose will be used as the active layer in a metal-insulator-metal (MIM) structure, with conductive carbon as top contact and platinum as bottom contact.

Therefore, for a better understanding, the main following objectives will be covered:

- Study of the electrical performance when vary the quantity of ZnO or/and EC in the active layer.
- Study of the electrical performance when vary the thickness of the active layer
- Study the influence of UV irradiation after deposit the active layer

The electrical characterization of the final devices after optimized the process, will be performed in order to understand their performance, and its switching mechanism. The characterization will focus the endurance and retention performance.

1 INTRODUCTION

Recent breakthroughs over the past years on the field of nanostructured ZnO, make it possible to incorporate it in several applications, from antibacterial antifungal agents in medicine to microelectronic, namely in transistors, diodes and memories. Figure 1.1 illustrates the application of ZnO nanostructures in some devices.

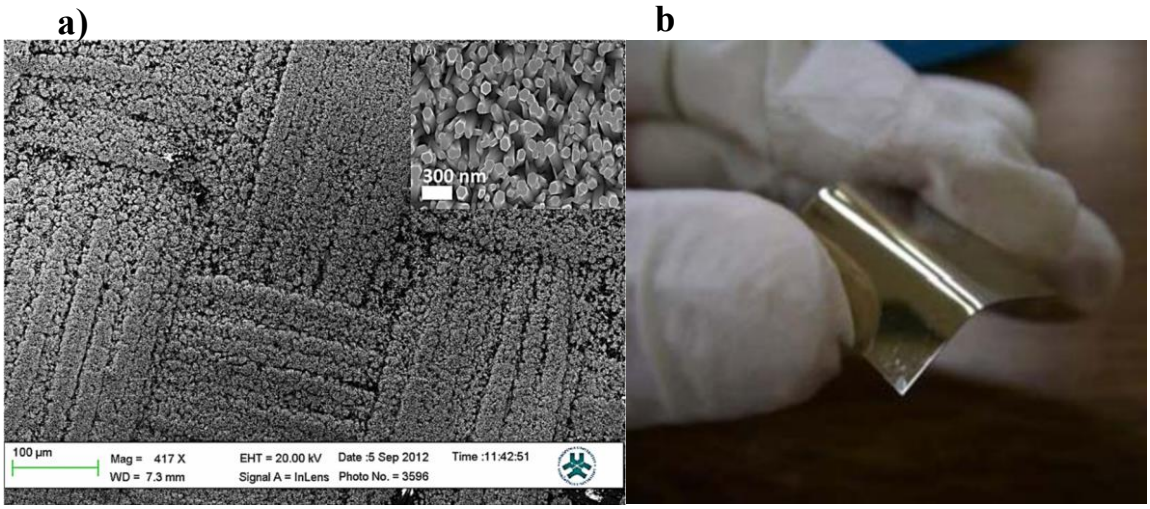

Figure 1.1 a) Application of a zinc oxide nanorods in textile substrate targeting the development of a diode [6] **b)** Zinc Oxide based memory on stainless steel substrate [7]

The studies and investigation conducted in order to understand the physical and electrical properties of this amazing material, make ZnO a well-established candidate for its subsequent integration in microelectronic devices, namely as a semiconductor [6, 8-10]. In the next sections, a brief introduction about paper substrates and memories, making a short state-of-the-art about fully-printed memories in particular of ZnO based ones. At the end it will be explained the screen-printing technique used to prepare the ZnO layers as well the ink formulation used in this work.

1.1 Paper as substrate

We are entering in an era where the resources are starting to be limited to respond our consumption demands. Cellulose could be the solution because it is the Earth's major biopolymer and is one of the most common and cheapest of all substrate materials used in our society. Most importantly it is recyclable and biocompatible [11]. There are several polymorphs of crystalline cellulose. Cellulose I is metastable and is naturally produced by a variety of organisms (trees, plants, tunicates, algae, and bacteria). Cellulose II has been the most stable structure of technical relevance and can be produced by two processes: regeneration (solubilisation and recrystallization) and mercerization (aqueous sodium hydroxide treatments). Cellulose III can be formed from Cellulose I or II through liquid ammonia treatments, and subsequent thermal treatments can then be used to form Cellulose IV [12]. There is also Bacterial Cellulose that has a crystallography structure similar to cellulose I, which is common with natural cellulose of vegetal origin. It consists a two cellubiose units arranged parallel in a unit cell and that cellulose molecules tended to have a specific planer orientation in dried film [13].

Due to the polar nature of cellulose and its porous structure, natural fibres are presently attractive supports for deposition and stabilization of nanostructured materials [13]. This functionalization can be achieved using a wide choice of cellulosic structures (whole fibres, micro- and nanofibers and nanocrystals), and nanostructured materials (noble metals, transition metal oxides, semiconductors). Applications of these materials range from energy storage, catalytic beds for pollutant capture and

degradation, new membranes, smart textiles, antimicrobial elements, screens for electronic applications, magnetic products and electrical devices such as diodes, transistors and memories [13], replacing expensive and rare materials used in electronics [11].

In comparison to traditional paper excellent optical transmittances, enhanced printable proprieties and higher tensile strengths are achieved in cellulose nanopapers (the bacterial cellulose used in this work has Cellulose nanofibers) [14-17]. Unfortunately, some of the functional properties of cellulose nanopapers such as ultraviolet (UV) permeability [17], stability against moisture [15-17] and thermal stability [18] still remain below the required standards for their commercialization in industrial applications [14].

1.2 Memories: from its most basic definition to RRAM

In the simplest way, a memory is an electrical device which is used to store information. It can be divided in two big categories: Volatile memory, that requires power to maintain the stored information which dynamic random access memory (DRAM) and static random access memory (SRAM) are the most used in computers. By the other hand, the non-volatile memory (NVM) retains the data if there is no voltage applied or by other words when the power is off. This thesis will focus on NVM. Today, Si-based Flash memory devices represent the most prominent NVM because of their high density and low fabrication costs. However, Flash suffers from low endurance (10^6 cycles), low write speed (> 1 µs [19]), and high voltages required for the write operations. In addition, increasing the density of Flash is expected to run into physical limits in the near future. Ferroelectric random access memory (FeRAM) and Magnetoresistive random access memory (MRAM) cover niche markets for special applications due to inherent problems in the scalability to achieving the same density as Flash today. To overcome the problems of current NVM concepts, a variety of alternative memory concepts is explored. Most notably, NVMs based on electrically switchable resistance have attracted considerable attention, called resistance (switching) random access memory, RRAM [20].

RRAM have attracted rapidly increasing attention for non-volatile memory (NVM) applications.[21, 22]. This type of memories should display characteristics such as high-density and low cost, fast write and read access (high-speed operation), low energy operation, and high performance with respect to endurance and retention. [23] Generally, a resistive memory is composed of a metal-insulator-metal (MIM) cell, where the NVM effect comes from their ability of reversible resistive switching (RS) between low-resistance state (LRS) and high resistance state (HRS) under application of a voltage sweep or a voltage pulse [24].

Among the various candidate active materials for RRAM, ZnO has promising advantages, such as facile synthesis, reversible and steady RS property, and low set and reset voltages [25-27]. Analysing the physical properties of ZnO it has high charge-carrier mobility, high optical transmittance, and good chemical/mechanical stability. Amorphous or polycrystalline ZnO have a direct bandgap (about 3.4 eV at room temperature), with a conduction band based on non-directional Zn 4s orbitals. This confers attractive physical properties, such as high isotropic electron mobility (higher than 1 $cm^2V^{-1}s^{-1}$) and low-temperature process ability, lower than 300 °C. This means zinc oxide could be used as semiconductor in paper substrates [10]. Due to the existence of intrinsic defects, such as vacancies at the oxygen sites (VO) and Zn interstitials (Zni), ZnO nanoparticles with a wurtzite structure are a natural n-type semiconductor.

Table 1 summarises some of the most important publications that have been made regarding the use of ZnO in memory devices and also the first fully-printed paper RRAM. Despite in all papers with exception of [28] the active layer was based on ZnO, the switching mechanism varies: from a formation of a conducting filament [7, 29, 30] to charge trapping-detrapping [31] or even hopping conduction [32]. With exception of [31] which is a write once read many times (WORM), they reported the existence both unipolar and bipolar switching. Bipolar happens when the RESET occurs at inversed voltage polarity compared to the SET process. By the other hand, unipolar switching happens when the set process which must have a compliance current occurs at the same voltage polarity than the reset process which happens in a lower voltage compared to the SET process with no compliance.

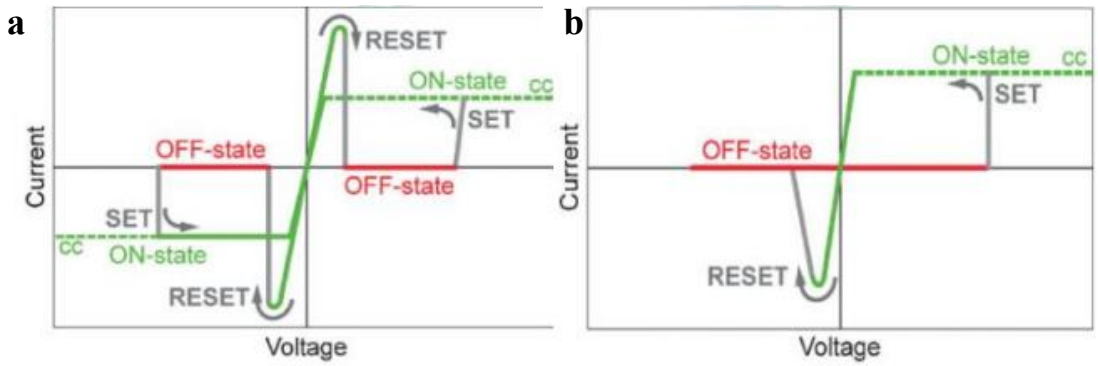

Figure 1.2 - **a)** Typical I-V curve of a unipolar **b)** and bipolar resistive memory, (adapted from [20])

Analysing the publication in table 1, it is evident there is a novel area where it lacks a development of a ZnO RRAM using low cost techniques and low annealing temperatures, in order to make it possible to be fabricated in paper substrates. Thus this work aims to fill this gap. It will aim to create a ZnO RRAM on a paper substrate using low cost printing techniques as possible with lower temperature annealing than 150 °C. ZnO can be processed and printed, using solution precursors. In this work ZnO obtained from sol-gel method [33] and commercial nanoparticles (NPs) will be explored in ways to work as the active layer in RRAM devices

Table 1.1-Key parameters of the reported RRAM i.e. the substrate, the active layer, the position technique, te anealing temperature, the electrodes and the endurance

YEAR	SUBSTRATE	ACTIVE LAYER	DEPOSITION TECHNIQUE	ANNEALING TEMPERATURE (°C)	ELECTRODES	ENDURANCE
2016 [29]	TiO2/SiO2/Si	Co:ZnO	Spin coating	550	Pt	50 cycles
2012 [30]	Ti/SiO2/Si	ZnO	RF sputering	RT	Pt	10^6
2009 [7]	Stainless Steel (SS)	ZnO	RF sputering	RT	Au top SS bottom	100
2016 [31]	PEN	ZnO:EVA	Thermal roll lamination technique	150	ITO	WORM - write only
2014 [28]	Paper	TiO2	Screen printing	180	Ag top C bottom	30 000 cycles

1.3 Screen Printing technique

Conventional techniques, such as chemical vapour deposition and sputtering, usually require vacuum and high-temperature conditions. Considering the fabrication environment and chemical compatibility, most of these fabrication processes are not suitable for paper-based device [28].Also, with increasing demands for more economic routes to manufacture electronic devices [34] and find fabrication methods that do not require high temperature process or annealing which is crucial when using paper substrates, various techniques for the fabrication of microelectronic devices, including screen printing, Nano-imprinting, ink jet printing, and direct printing, are generating an increasing interest.

In this work screen printing technique was chosen to fabricate 2 of the 3 layers which constitutes the device. However, the platinum bottom contact was deposited using E-beam evaporation, an expensive fabrication process compared to the low cost screen printing technique. Despite the possibility of printing platinum using Heraeus Silica and Metals, RP10001-145B ink, the required high annealing temperature impossibilities the use of paper substrates [35, 36]. The platinum is dispersed within an

organic resin which is completely burnt off during the firing process producing metal films of high purity. The temperatures required achieves 850 °C which is completely incompatible with paper [35, 36].

Screen printing, in which screen masks are used to deposit materials onto large-area substrates with high throughput, is considered as one of the scalable printing techniques and has been widely used in printed electronics. Benefiting from its simplicity, scalability and environment-friendly process, this technique shows tremendous potential for mass production of large-area electronics at very low cost [37]. In addition, screen printing allows patterning (to define which areas of the substrate receive deposition [38]).A basic concept of screen printing consists in applying pressure to the squeegee, it moves over the screen. When the squeegee enters in contact with the ink, it creates shearing stress to the ink and the viscosity is decreased. Then, the ink is transferred, in a controlled manner, through the apertures of a mesh and deposited on to a substrate. Any required pattern can be printed by blocking off appropriate mesh apertures with a photo emulsion layer to form a printing screen. The pattern definition is also dependent on the mesh count (number of threads per inch) [39]. An important parameter to control is the ink viscosity, that should be low enough for easy flow through the mesh under the shearing stress, but high enough to keep its form when deposited, and with the shearing stress removed, to prevent lateral flow. Viscosities, typically between 500 - 5000 cPs are referred to as desirable for this technique. Also, printing speed, angle and geometry of the squeegee, mesh size, material, strength and snap-off (distance between screen and substrate) are main factors to consider in order to achieve high-resolution patterning (30 - 50 µm), through this printing technique. In figure 1.3, is displayed a schematic draying of the used screen-printing present in CENIMAT|I3N.

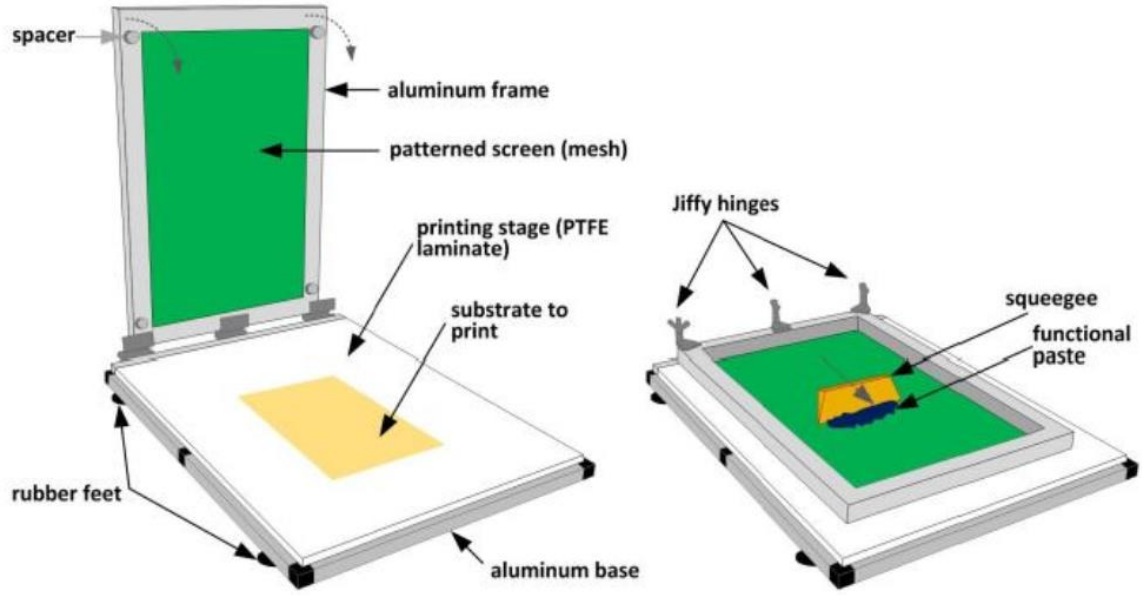

Figure 1.3 - Schematic representation of the custom-made screen-printing present in CENIMAT|i3N[40]

1.4 Ink formulation for RRAM fabrication

Considering the importance of developing an ink that should have the ideal viscosity to achieve a high quality printing, this subsection will give an explanation of the selected materials for the ink development.

To successfully formulate a nanoparticle thick film, the ink must be developed by using raw materials that do not compromise the desired application. The ink must be prepared dispersing the chosen inorganic powders/precursors in a viscous liquid, the vehicle, which is responsible for the deposition of the powder onto the substrate. Both of these components must be dispersed along with an organic or sacrificial binder with a solvent and a wetting agent.

For this, resin or polymeric binders such as cellulosic polymers, as is the case of ethyl cellulose (EC) is widely used for industrial screen-printing as it provides good printing and levelling [41]. The sacrificial binder is used in order to hold the inorganic powders together and give the ink the intended rheological properties [42]. Additionally, solvents with low vapour pressure at room temperature and a high vapour pressure at 100 – 150 °C, should be selected, in order to prevent ink drying by evaporation on the screen and enable rapid drying of the printed parts by annealing. Another reason for choosing EC is due to the fact that EC act as an insulator due to its low electronic conductivity [41] which is crucial to the memory effect.

2 MATERIALS AND METHODS: FABRICATION, OPTIMIZATION AND CHARACTERIZATION OF ZnO RRAM DEVICES

The following chapter will present all the steps to develop, characterize and optimize the RRAM devices based on ZnO NPs. First it will be focused on the inks formulation that will be used as active layer. Next, it will be shown the architecture chosen for ZnO RRAM devices, explaining as well the several steps and techniques used for all of the layer depositions. At last, it will be listed all the characterization techniques selected to study the morphology and structure of the active layer, i.e. the ZnO nanoparticles dispersed into a cellulose matrix based on ethyl cellulose. Finally, the electrical characterization conducted for each device will be presented.

2.1 ZnO ink formulation materials and reagents

The methods adopted for preparing the active or semiconductor layer ZnO NPs screen printing paste, i.e. the ZnO nanoparticles dispersed into a cellulose matrix based on ethyl cellulose were based and adapted from the literature [43].

The binder solution was prepared by dissolving 5% wt EC 300 cP ($C_6H_7O_2(OC_2H_5)_3$; CAS: 9004-57-3) from Aldrich on an 80:20 toluene/ethanol solution ($C_6H_5CH_3$; CAS: 108-88-3 / C_2H_6O; CAS: 64-17-5). For its complete dissolution it should be 12 hours under stirring at 600 rpm.

Then, three different inks were synthetized, as depicted in table 2.1, in order to optimize the device and also to understand the role of ZnO, EC.

Table 2.1 - Inks composition developed in this work and its quantity

	ZnO concentration (%)	ZnO mass (g)	Toluene/Ethanol + 5%EC mass (g)
A	0	0	10
B	10	1	9
C	40	4	6

2.2 ZnO:EC RRAM by screen-printing

The architecture adopted in this work consists in the active layer sandwiched between two different contacts, as shown in the schematic representation, figure 2.1. In order to decrease the factors that could influence the RRAM behaviour, one of the electrodes must be inert and platinum was the chosen material. To keep the fabrication simple, a 100 nm thick platinum layer was deposited over 20 nm of titanium, to ensure the adhesion to the paper substrate. Both metals were deposited by E-Beam evaporation. The remaining layers were printed using a homemade screen-printing system described on figure 1.2

Before printing the active layer, the paper with platinum already deposited, should be subjected to an ultraviolet (UV) irradiation during 30 min through a UV-Ozone Cleaner – Novascan PSD-UV. After finishing the surface cleaning process, the semiconductor layer was printed through a mesh model 77-55 (mesh count 190, aperture 81 µm and thread diameter 55 µm), followed by 2 min annealing on a hotplate at 120 °C. Finally, some devices were also exposed for 15 min to UV irradiation.

At last the top contact pattern (defined in figure 2.1) was printed using a mesh model 120-34 (mesh count 305, aperture 45 µm and thread diameter 34 µm), followed by 2 min annealing on a hotplate at 120 °C. For the top contact two different inks were tried: silver ink (PE-AG-530 ink, Flexible Silver Conductive Ink) and carbon ink (PE-C774, Carbon Resistive Ink), both from Conductive Compounds, Innovative Chemistry for High Tech Applications

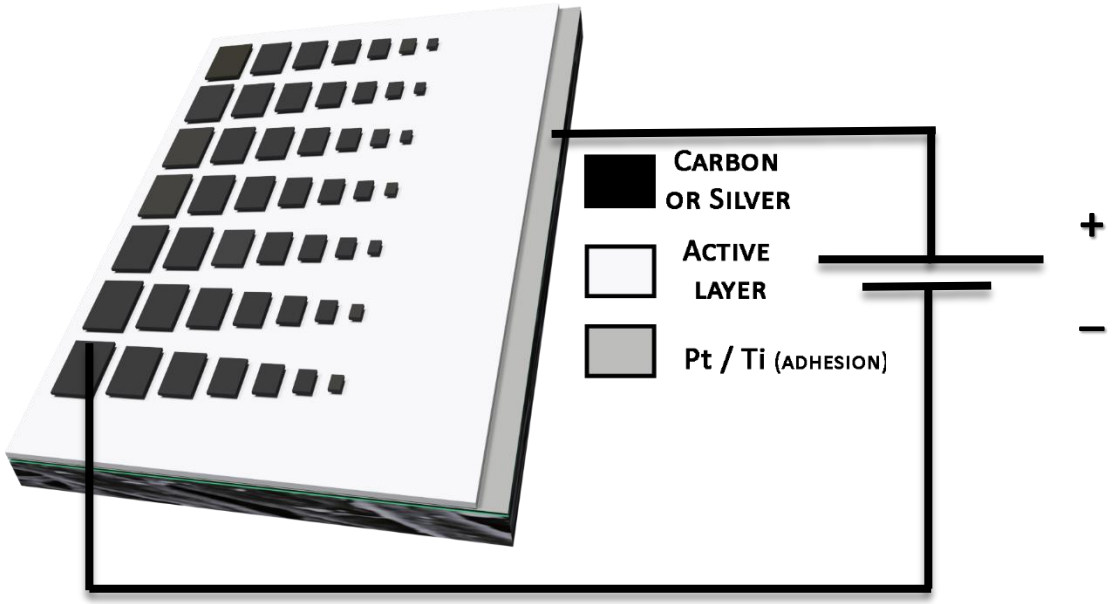

Figure 2.1 Schematic representation of the architecture adopted in this work and their conections to the Agilent B1500A Semiconductor parameter analyzer

2.3 ZnO RRAM using printing pen

The architecture adopted is similar to the devices fabricated in subsection 2.2. This approach was used in order to get the active layer consisting only of ZnO nanoparticles, since the ink here used do not require high viscosity, hence the EC binder as used for screen-printing patterning. Here, the semiconductor layer was drawn using the Pen on Paper technique where we selected a parallel plate nib pen from Pilot and ZnO dispersion (50 wt. % in water) from Aldrich (CAS: 721077-100G) as the semiconductor layer. This semiconductor layer was dried at room temperature and in order to study the influence of its thickness and the number of printing steps were from one to three.

2.4 Characterization techniques

The active layers used in the devices were characterized by Scanning electron microscope (SEM) using the Hitachi TM 3030Plus Table Top Scanning electron microscope for cross section in order to determine the estimate thickness of the screen-printed layers.

Fourier transform Infrared (FTIR) spectroscopy was applied in order to evaluate the effect of UV irradiation on the semiconductor layer. The 40% ZnO ink was screen-printed on glass substrates, previously cleaned in acetone, IPA and DI water. The spectra were acquired between 4500-500 cm^{-1}, using a Nicolet 6700 FTIR Thermo Electron Corporation device.

Leica IC80 HD microscope and the LAS V4.3 software were used to measure the top contact dimensions.

The electrical characterization of the resistive memories was performed at room temperature using an Keysight B1500A semiconductor parameter analyser connected to a Cascade Microtech EPS150 manual microprobe station, controlled by the software Keysight Easy Expert. As depicted in figure 2.1, the bottom electrode was connected to positive bias and the top electrode was grounded.

3 RESULTS AND DISCUSSION

In this work, several devices were tested in order to study the influence of the active layer composition and thickness, as well the UV influence and the use of silver top electrode was studied for the 40%ZnO: EC. Table 3.1 resumes the fabricated devices characteristics and their nomenclature from here on out.

Table 3.1 – All fabricated devices characteristics and their nomenclature

Name	Composition	Printing technique	Printing steps	UV irradiation	Top Electrode	Bottom electrode	Substrate
EC	Only EC (A)	Screen-printing	2	✓	Screen-printed Carbon	Screen-printed Carbon	Paper
ZnO1 ZnO3	Only ZnO	Pen Drawing	1 3			E-beam Platinum	
10ZnO	10%ZnO+EC (B)	Screen-printing	2				
40ZnO1	40%ZnO+EC (C)	Screen-printing	1				
40ZnO2C							
40ZnO2Ag			2	✓	Screen-printed Silver		
40ZnO3			3	✓	Screen printed Carbon		
40ZnO3no UV				×			

In this section it will be reported and discussed the electrical characterization of each modification introduced. The main objective in these study is to develop the suitable ink for resistive memory switching and the optimization of the fabrication methods i.e. active layer printing steps, the use or not of UV irradiation after the deposition of the active layer and the electrodes material. At the end, it will attempt to find a suitable mechanism for the memory effect on these devices.

3.1 Study of memory effect when using only ZnO NPs as active layer

Using screen-printing technique is almost impossible to print ZnO without binder, so it was chosen drawing pen technique to draw lines consisting only of ZnO with the intention to comprehend the importance of ZnO itself and also if EC is having an important role to the memory effect. The architecture adopted consists in bottom platinum contact and screen-printed carbon top electrode. Figure 3.1, shows the surface of

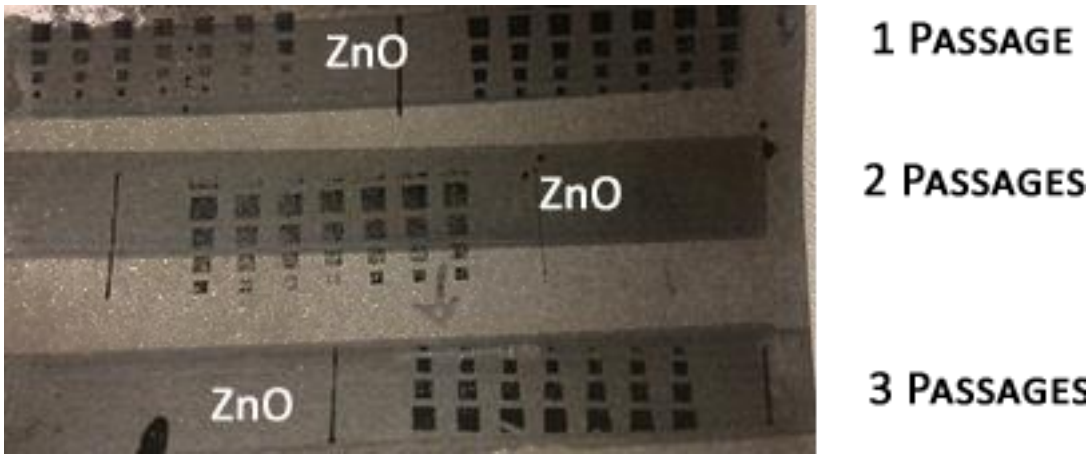

Figure 3.1 - Image of the surface of drawn ZnO lines with different number of passages between screen-printed carbon top contacts and E-beam platinum bottom contact on paper substrates

Figure 3.2 resumes the electrical characterization of these devices without compliance (delimited by equipment limitation) and using 200 ms of delay time, 100 mV of step size. For one writing pen passage (ZnO1), it is evident the hysteresis is low and despite of having some memory effect, it only achieved one cycle, where the first run in green, the device switched from LRS to HRS (RESET) at -20 V and at the second run in blue, the device switched from HRS to LRS (SET) at 25.2 V. The difference between LRS and HRS around half order of magnitude which is too low to distinguish the two resistance states. Also the device remained stable after 100 s reading at 500 mV. As well, the resistance of the device is 21 kΩ.

Figure 3.2 b) shows the electrical characterization of one device, when the number of pen passages is increased to three (ZnO3). It was made two I-V sweeps: the first one from -5 V o 5 V in blue and the second from -10 V to 10 V in magenta. In both curves, the hysteresis is completely disappeared, acting a resistor. Moreover, the resistance increased one order of magnitude to 241 kΩ due to increase of ZnO thickness.

With this experiment, using only ZnO in the active layer, it had low hysteresis. Thus, the presence ethyl cellulose seems to plays a crucial role to the memory effect.

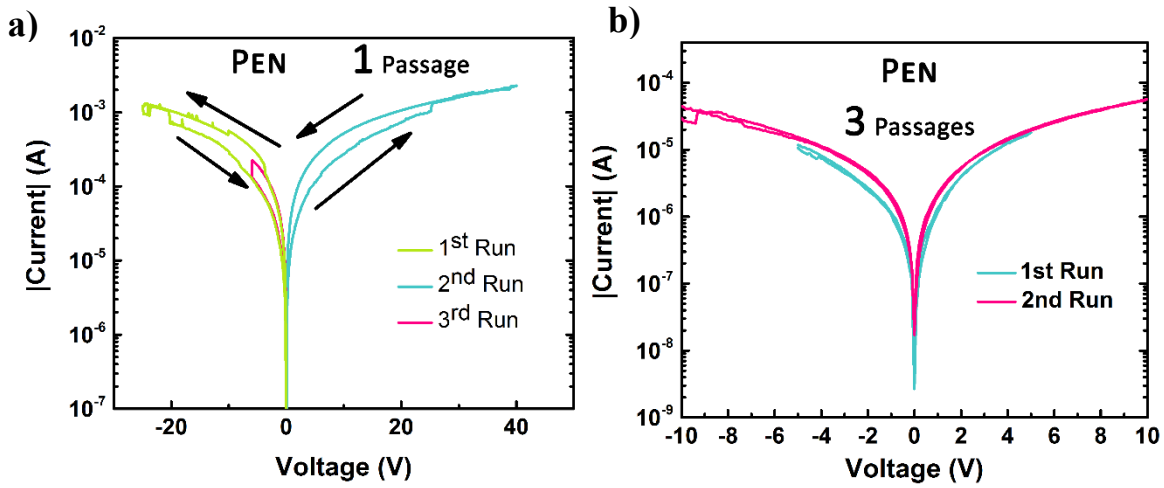

Figure 3.2 - I-V curves of ZnO between carbon top contact and platinum bottom contact on paper substrate for: **a)** one writing step **b)** three writing steps

3.2 Study the memory effect of EC as active layer

Figure 3.3 shows the initial I-V sweep from -5 to 5 V on a fully-printed structure using only EC as active layer (2 printing steps of screen-printed EC between screen-printed carbon electrodes), showing that the device is in a high current state due to its high current reaching 1 mA at 2 V. So the next step consists in performing a RESET.

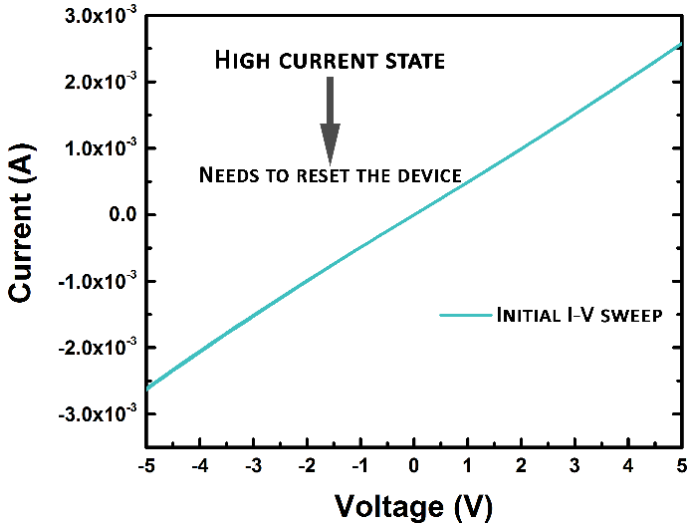

Figure 3.3 - First IV sweep realized during electrical characterization, showing a device in LRS

Figure 3.4 resume the I-V sweeps made as well the reading tests at 500 mV for 10s. The steps 1 to 3 correspond to a successful attempt to RESET the device, where a voltage sweep was made from 0 to -40 V, with a delay time of 500 ms, a step size of 100 mV and a current compliance of 0.1 A. Using this structure, the first RESET switch occurred at very high voltage, at -27.2 V with a current of 35.7 mA. However, at -2 V the current raised and it came to an intermediate current state.

The steps 4 to 6 correspond to a SET switch. Nevertheless, at 2.2 V the current drop to an intermediary current state to a lower current state and at 9.8 V the device was SET, reaching the compliance of 100 µA. Then the device was erased (step 7) and the voltage value dropped to -2 V when compared to the 1st cycle. However, the device never returned to LRS, achieving only one cycle. One reason to the poor performance could be related to the ink viscosity. As the ink does not contain ZnO, which it adds viscosity to the ink itself, the viscosity is too low to ensure a good deposition.

Due to low endurances cycles is not considered as a reliable memory. Thus it could be for two reasons: the formation a carbon filament due to redox reaction on the electrodes (electrochemical memory) in the presence of ethyl cellulose. The literature does not support the conductive bridge memory effect since carbon is inert [28]. Also using conductive carbon (it was used a conductive carbon ink) the current density needed for form a filament is 350 MA/cm^2 [44]. Since the area of the smallest electrodes used is 2.5 x 10^{-3} cm^2 and the maximum current of the characterization equipment is 0.1 A, the theoretical maximum current density that could achieve is 40A/cm^2, five orders of magnitude below needed to form a carbon filament. Therefore, fabricate these devices revealed that EC has a crucial role to the memory effect.

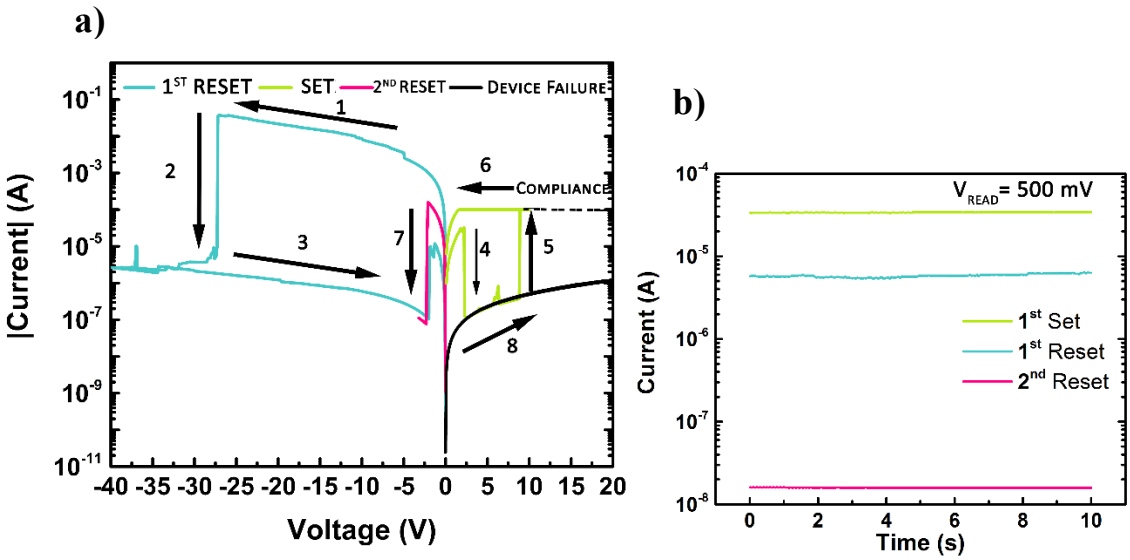

Figure 3.4 - a) Endurance cycles performed of EC between carbon top and bottom contact on paper substrate **b)** Reading tests for 100 s at 500 mV after the SET and RESET the device

3.3 Study the memory effect when using 10% ZnO with 5 % EC as active layer

RRAM on paper substrates were fabricated using an ink that contains 10 % wt ZnO with 5% wt EC, between an E-beam deposited platinum and screen-printed carbon or silver electrodes. As depicted in figure 3.5, making a visual inspection of the substrate fabricated, it is visible the lack of uniformity of the active layer, even after two printing steps. Looking only for the platinum and the active layer, the darker zones of the device correspond the screen-printed active layer while the lighter areas, especially in top left of the device, suggest the active layer is not present. The cause of poor printing process could be attributed to the clogging of the mesh causing the lack of uniformity. However, a visual inspection to the mesh used to print the active layer didn't show any signs of obstruction. The other reason that could be caused the poorly printed active layer is related with the low viscosity of the 10 % wt ZnO ink that do not allow for good film formation.

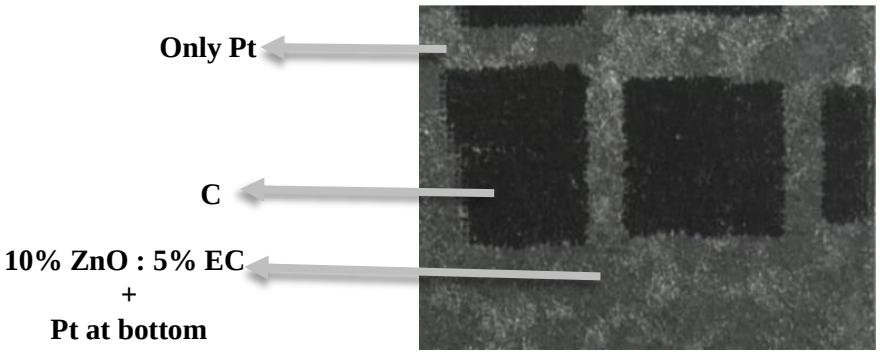

Figure 3.5 - Image of the surface with screen-printed 10% ZnO : 5% EC layer with carbon top contacts on paper substrates

Electrical characterization was performed on this substrate. The positive bias was connected to the platinum electrode and the carbon contact was grounded. Figure 3.6 shows the initial I-V curve from 0 to 3 V. In this range of voltage, the current is lower than 100 nA, meaning the device is virgin and it needs an electroforming process.

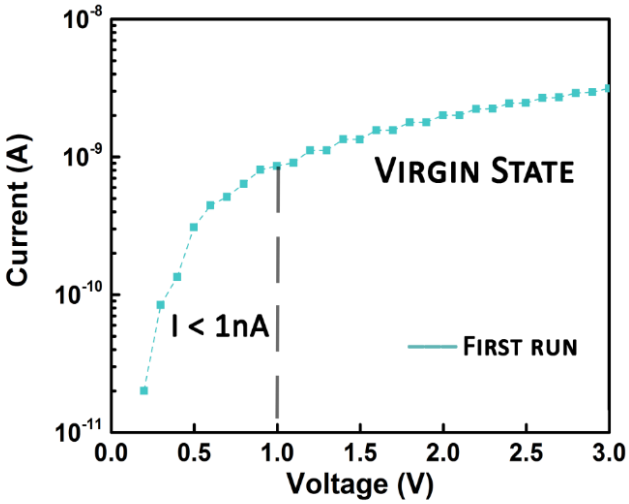

Figure 3.6 - First I-V sweep realized during electrical characterization, showing a virgin device

The next step consists to perform an electroforming process. Figure 3.7 a) shows I-V curves for the electroforming process in magenta and its erase in blue. The steps 1 to 6 represents the electroforming process which it consists to switch from high resistance state (low current) to a lower resistance state (higher current). At 5.6 V the device changed from HRS, where the current is below 10 nA, to LRS, reaching current values around 1 mA. Next, as shown in figure 3.7 b), it was made a reading test for 100 s at 500 mV to ensure the device was at LRS. At 500 mV, the current is 19 µA and it remained stable over 100 s. Subsequently, it was performed the RESET switch, or erase process. The steps 7 to 11 represents the RESET switch, that occurred at -10.3 V and reaching a current of 1.3 mA. Making a reading after RESET the device, the current dropped to values below 1 nA. Thus, the difference between the two states is at least four orders of magnitude.

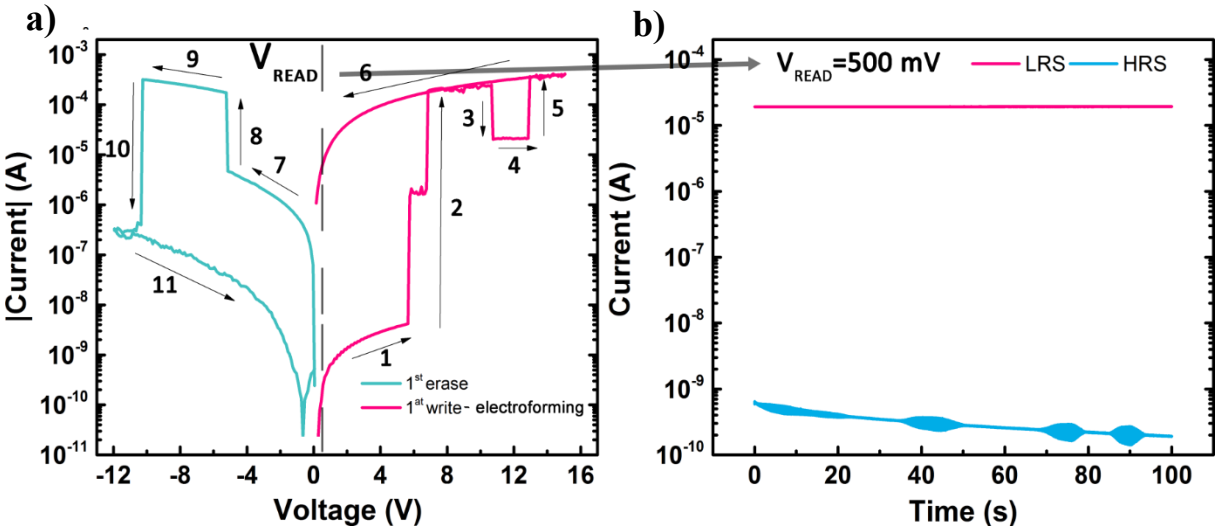

Figure 3.7 - a) First cycle performed on 10 % Zno : 5 % EC with carbon top contact and platinum bottom contact (10ZnO) **b)** Read test for 100 s at 500 mV after the first SET and RESET the device in a)

Figure 3.8 shows the 2nd cycle, initially making I-V sweep to positive voltages in order to SET the device. However, even make I-V sweeps in both sides, the current value remains low, below 1 µA, which it means the change did not occur and it remains at HRS. The noise associated could indicate a competition between formation and rupture of the conductive filaments by the current itself.

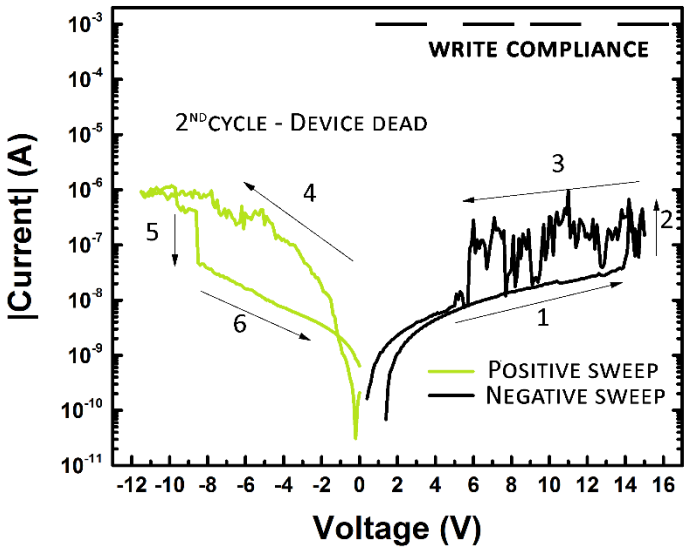

Figure 3.8 - Second cycle performed on 10 % Zno : 5 % EC with carbon top contact and platinum bottom contact (10ZnO)

Thus, using the ink that contains 10 % ZnO, it only managed one cycle. The percentage of ZnO could not be enough and the higher EC/ZnO ratio could lead to instability. Nevertheless, it is crucial to perform more tests to confirm the hypothesis. Also as seen in figure 3.5 the printing quality were poor due to the low viscosity of the ink and as result several devices were short circuited.

3.4 Study the memory effect when using 40% ZnO with 5 % EC as active layer

As discussed in subsection 3.3, the biggest problem concerning the endurance of the memories when using a ZnO concentration of 10 % could be related to the low viscosity in the ink and some instability caused by the high EC/ZnO ratio. Therefore, one solution consists in increasing the concentration of ZnO, which it increases also the ink viscosity. Consequently, it was made several devices using 40% ZnO: 5%EC ink, where several factors were changed in order to optimize the device as depicted in table 3.2: the number of printing steps, the UV irradiation after screen-printing the active layer and the use of silver top electrode instead of carbon.

Table 3.2 - Device characteristics using 40% ZnO ink

Name	Active layer Composition	Printing technique	Printing steps	UV irradiation	Top Electrode	Bottom electrode	Substrate
40ZnO1	40%ZnO+EC (c)	Screen-printing	1	✓	Screen-printed Carbon	E-beam Platinum	Paper
40ZnO2 C			2	✓			
40ZnO2 Ag					Screen-printed Silver		
40ZnO3			3	✓	Screen printed Carbon		
				×			

3.4.1 UV irradiation influence on the active layer

The study of the influence of the UV irradiation after deposition of the ZnO:EC layer was realised by ATR-FTIR. The 40 % ZnO : 5 % EC ink was screen-printed on glass substrates and annealed at 120 °C. The difference consists in one sample was UV irradiated for 15 minutes and the other sample was not irradiated.

In figure 3.9 shows the ATR-FTIR spectrum for the ink with these two distinct treatments performed. For EC, the peak at 3500 cm^{-1} represents the stretching of O-H groups both in the closed ring structure and in intra/intermolecular hydrogen bonds. The peaks around 2980-2870 cm^{-1} may indicate CH stretching and the distinct peak at 1375 cm^{-1} refers to CH_3 bending. As well, the small peak at 1440 cm^{-1} represents CH_2 bending, and the broad peak around 1100 cm^{-1} might be due to C-O-C stretching in the cyclic ether [45]. In both samples it is evident the presence of the EC, which it means the EC do not degrade when exposed to 15 min of UV irradiation. Additionally, the decrease of intensity at 3500 cm^{-1} and at 1100 cm^{-1}, when submitted UV irradiation could be related the loss of toluene and ethanol that did not fully evaporate during annealing.

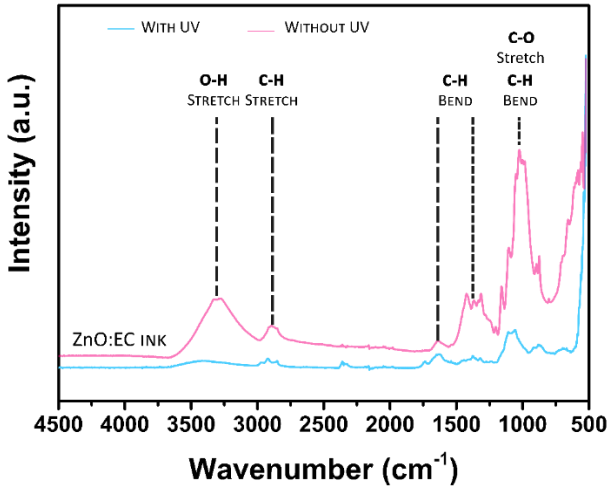

Figure 3.9 - ATR-FTIR spectra of the ZnO NPs:EC ink after being screen-printed on a glass substrate and submitted or not UV irradiation for 15 min.

Figure 3.10 shows the electrical characterization of the best device not submitted to UV irradiation. Electroforming process was necessary to preform since the device was virgin (an example is shown in fig 3.6). The device switches from HRS to LRS at 14.5 V. The RESET voltage increased over the cycle: from -3.9 V at 1st cycle to -10 V at 5th cycle. The SET occurred from 4.8 to 14.9 V, which is higher than the electroforming process occurred. Thus it is a sign of non-conventional bipolar behaviour.

In figure 3.11 a) where is depicted the endurance tests, it is evident the poorer performance, compared to devices that was submitted UV irradiation (40ZnO3): the resistance in HRS severely decreases, which is at least two orders of magnitude lower compared when making UV irradiation after printing the active layer (40ZnO3 devices). Also, the best device only performed five cycles before it enters in breakdown compared to twenty cycles achieved when use UV irradiation after printing the active layer.

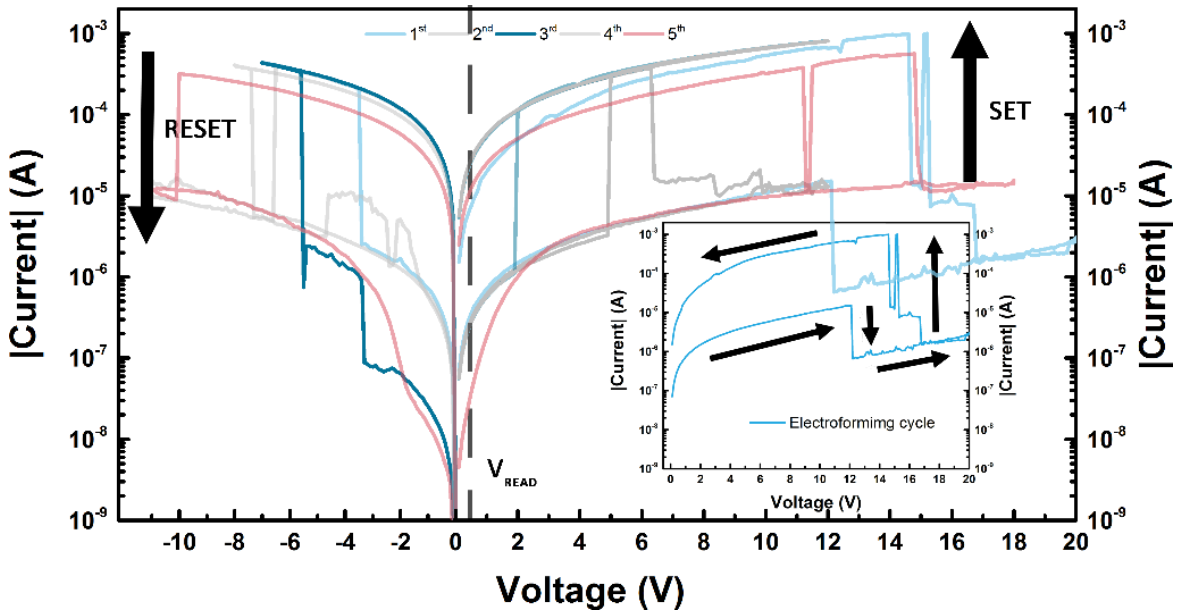

Figure 3.10 - Endurance cycles performed on 40 % Zno : 5 % EC with carbon top contact and platinum bottom contact on paper substrate without UV irradiation

Most important, in figure 3.11 b) was performed a retention test, for 1500 s at 500 mV. At 1450 s the current in LRS started to drop two orders of magnitude, from 10.5 µA to 100 nA, showing a sign of instability. Thus, it might conclude that making an UV irradiation after printing the active layer the memory become more stable. UV irradiation facilitates photodecomposition or photoreaction of ZnO into Zn^{2+} [46] creating more oxygen vacancies. As consequence, the devices that were submitted UV irradiation achieved better performance due to the elimination of solvents in the substrate that could cause electrical failure and the creation of Zn^{2+} radicals that induce more carries.

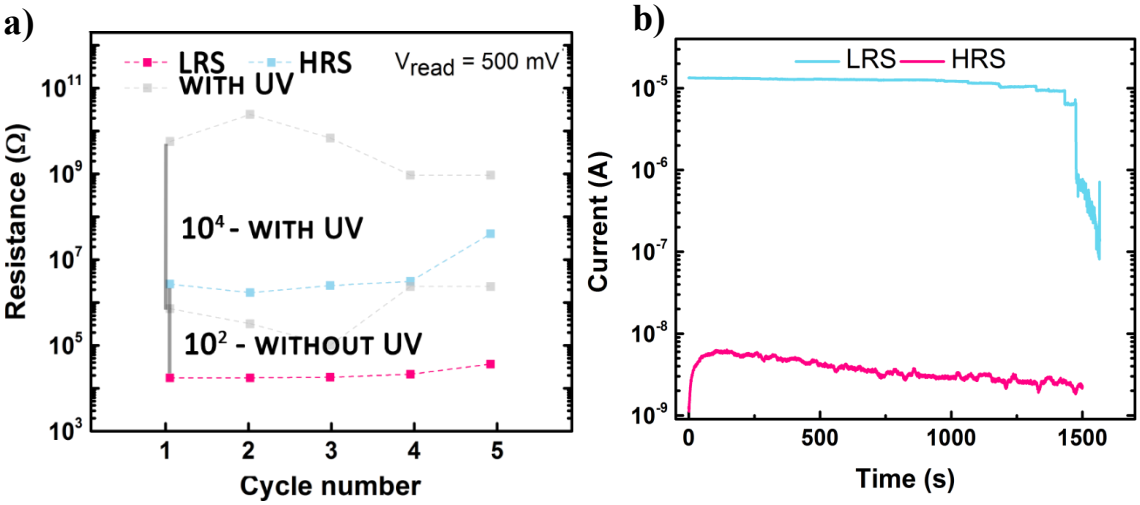

Figure 3.11 - a) average level of resistence at HSR and LSR after the SET and RESET the device in 3.10, comparing to a device that was made UV irradiation after printing the active layer **b)** Reading retention for 1 500 s at 500 mV after SET and RESET the device

3.5 Study the influence of active layer (ZnO:EC) thickness

The manual screen printing stage used in this work does not allow for a very accurate process. as seen by visual inspection of the fabricated devices in figures 3.14 and 3.19. So, it was crucial to check the layer uniformity in order to estimate the thickness, especially the ZnO mixed with EC layer which is crucial to the memory effect. One method to estimate the layer thickness is profilometry. However, this is not an adequate method due to the reasons listed: profilometry can only be used in smooth substrates and paper has high surface roughness. Also the active layer is delicate. Even using low force, when the tip makes pressure to the surface, it damages the layer. Using a glass substrate could be a solution to the first issue, but its more relevant to understand the deposition uniformity on paper substrate due to the high roughness. So making cross section of the devices produced and analysing using a SEM equipment would be important to understand the deposition uniformity and as important, to relate the thickness of ZnO with EC layer with the device performance.

The cross sections were made after performing electrical characterization, using liquid nitrogen in order to brake the cellulose fibres, avoiding smashing them, unlike the cuts made using scissors and razors. Four cross sections were performed in different substrates where the only difference was the number of ZnO + EC passages from a single printing step to three printing steps. All the SEM images have a magnification of 800 x and were edited using software *Photoshop cc 2015* by Adobe.

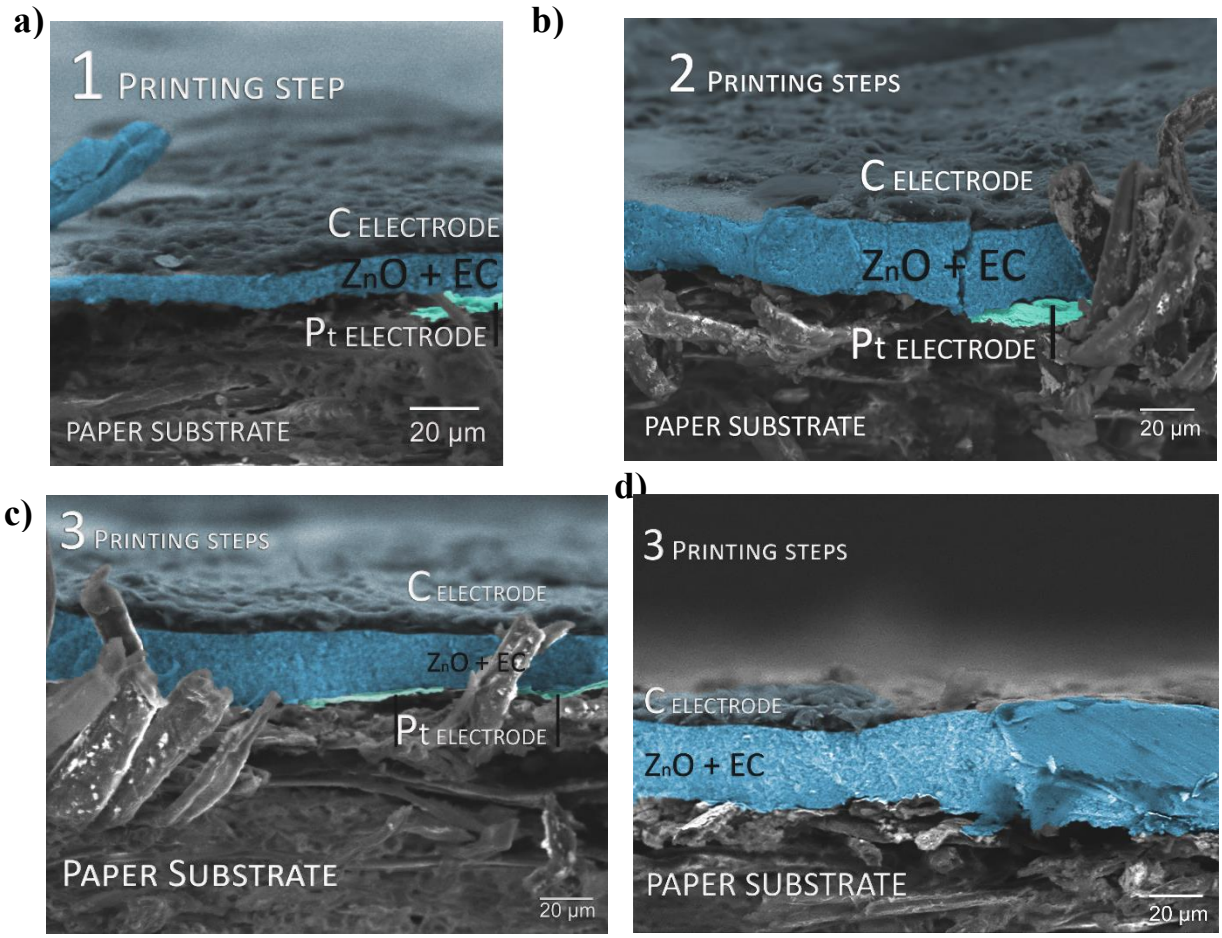

Figure 3.12 - SEM images of device cross sections with 800x of magnification and the ZnO:EC thickness over the distance graphic: **a)** with 1 printing step **b)** with 2 printing steps **c)** with 3 printing steps **d)** with 3 printing steps on another local

On SEM images in figure 3.12 all the layers are visible even the 100 nm thick platinum. Each layer was colorized using blue tones, which it can be used to easily distinguish them. The graphics of each image shows the carbon and ZnO plus EC thickness across the image when twenty measurements were made on each layer. It is evident that the ZnO with EC layer is not uniform over the image. This conclusion is expected because even perform a visual analysis at naked eye to the substrates the change of opacity is a strong evidence of non-uniformity of the layer. Also the average thickness of carbon in all conditions is 8.00 µm with a standard derivation of 2.20 µm which is perfectible acceptable for a screen-printed process. On the other hand, for ZnO mixed with EC layer the layer thickness rises with the increase of the number of printing steps: from one printing step the thickness is 9.37 µm with a standard derivation of 2.07 µm, for two printing steps the average thickness is 26.34 µm with a standard derivation of 3.40 µm. For three printing steps it was measured in two different locations on the substrate: one has an average thickness of 22.29 µm with a standard derivation of 2.12 µm (figure 3.12 c)) and another have average thickness of 30.37 µm with a standard derivation of 4.64 µm (figure 3.12 d)). Discussing this data leads the ZnO + EC layer is not uniform, varying form 22.29 µm to 30.37 µm, an increasing of 36 %. Another inconsistency is the ZnO + EC layer thickness for two printing steps is higher than having three printing steps. This could be justified for 3 printing steps the ink didn't pass through the mess creating a non-uniform deposition. Also for two printing steps, the zone where the cross section was made, it could have deposited a big amount of ink, creating a thicker layer. Thus it reveals the biggest issue of the manual screen-printing process: lack of uniformity over the film. This problem is related with the inconstant application of force through the squeegee or printing speed applied by the operator.

3.5.1 Comparison of electrical performance for different active layer thickness

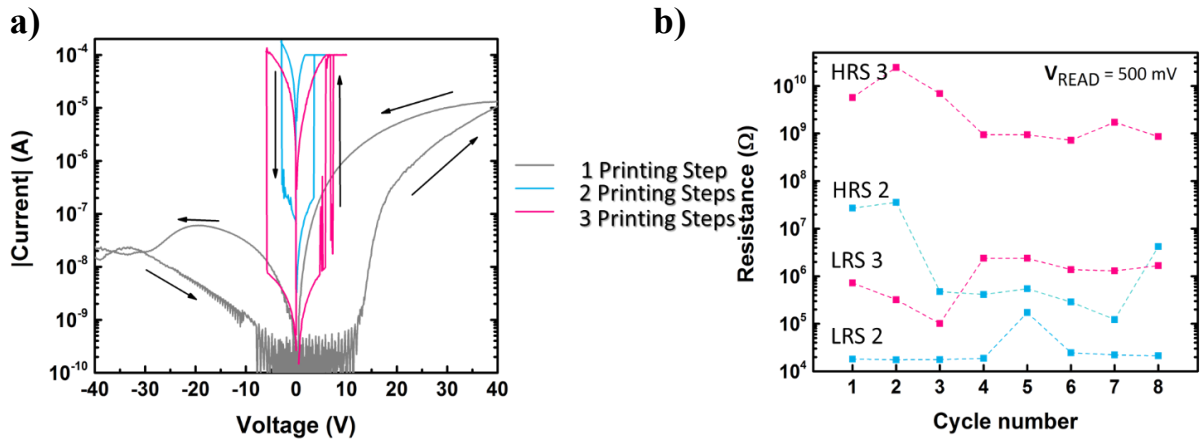

Figure 3.13 - a) 2nd cycle of 40ZnO1C, 40ZnO2C and 40ZnO3C; **b)** HRS current over the cycles for two printing steps and three printing steps of ZnO:EC layer

In figure 3.13 relates the performance of each device for different printing steps. In figure 3.20 a) is depicted the I-V curves made on 2nd cycle for two and three printing steps and as well a typical behaviour when has one printing step. The 40ZnO2C and 40ZnO3C have similar behaviour, but using three printing steps the hysteresis is higher. In figure 3.13 b) is evident the higher memory window at least one order of magnitude compared to two printing steps. This could be explained to increasing of thickness more isolate the layer become in HRS, meaning lower current in this state. However, there is a drawback. The voltage needed to set the device is bigger or the delay time should be increased.

For one printing step the behaviour is different. It shows hysteresis but there is not any abrupt change of current. In the positive voltage the current level when made the forward sweep (0 V to 40 V) is lower than backward sweep (40 V to 0). At negative voltages it is the opposite: the current level when

made the forward sweep (0 V to -40 V) is higher than backward sweep (-40 V to 0). Further investigation should be carried in order to understand this behaviour.

3.5.2 Two printing steps of 40% ZnO:5% EC with silver top contact (40ZnO2Ag)

As shown in figure 3.14, after two printing steps (40ZnO2C), the homogeneity of the active layer is acceptable. As well, the thickness in the right side of the substrate is lower, due to the decrease of opacity. Thus with two passages the 40% ZnO : 5% EC layer has an opaque white colour due to the higher amount of ZnO present in this synthetized ink.

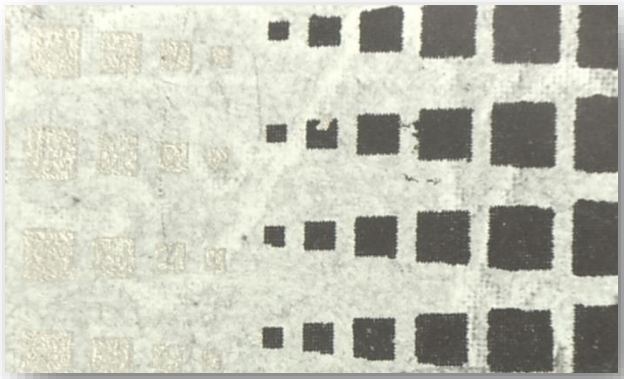

Figure 3.14 - Image of the surface with screen-printed 40% ZnO : 5% EC layer and also silver and carbon top contacts on paper substrates

Figure 3.15 shows the electrical tests performed in the best performance device in this substrate. All I-V sweeps used a delay time of 200 ms, a current compliance of 0.1 mA for the write process, a voltage step of 100 mV.

Analysing the cycles endurance (figure 3.15 a)), it was achieved seventeen full cycles, considering that the device did not write successfully on 18^{th} cycle. In colour, is represented some cycles (2,3, 10 and the last) where the device was programed in bipolar: the SET occurs at positive voltages the RESET occurs at negative voltage.

As depicted in figure 3.15 b), the switching probability of the SET and RESET over the voltage is calculated using the data obtained by the I-V sweeps made. The device transited from HRS to LRS (SET) happened in the interval of voltage from 2.5 V to 6.8 V and transited from LRS to HRS (RESET) occurred in the interval of voltage from -2 V to -9 V. As important, the voltage that occurred the resistive switches does not follow any tendency (increasing or decreasing) over the cycles. Annex A contains the switching values for each cycle.

Figure 3.15 c) depicts the resistance value of LRS and HRS after SET and RESET the device respectively. This test is important to verify if the change of resistance were successful. Moreover, with exception of 5^{th} and 18^{th} cycle, the average LRS value is 24 kΩ ± 5 kΩ and the average HRS value is 5 MΩ ± 10 MΩ. In opposite to the constant values of LRS, the values of HRS vary from 123 kΩ at 7^{th} cycle to 35.9 MΩ at 2^{nd} cycle. Also important with exception of 5^{th} and 18^{th} cycles, the difference between HRS and LRS is at least one order of magnitude which is enough to distinct the two states. However, at 5^{th} and 18^{th} cycles, the resistance value in LRS is inferior to the highest HRS value, which it means at these cycles the device was not written properly.

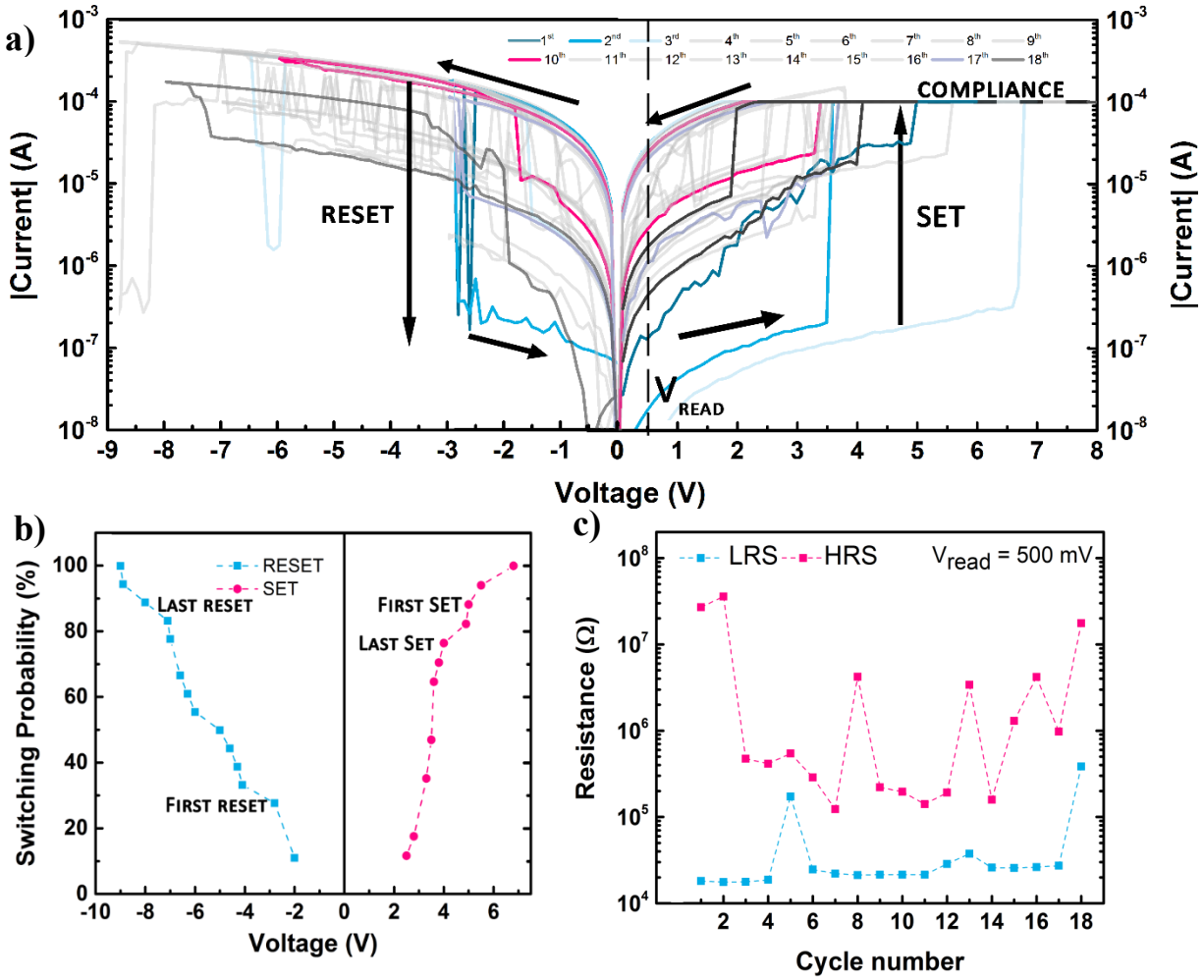

Figure 3.15 - a) Endurance cycles performed on 40 % Zno : 5 % EC with carbon top contact and platinum bottom contact on paper substrate **b)** Switching probability over voltage **c)**average LRS and HSR current after the SET and RESET the device in a) for 18 cycles

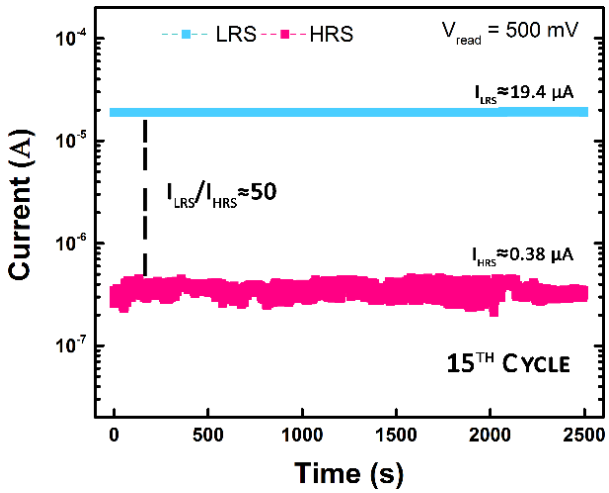

Figure 3.16 - Retention test for 2500 s at 500 mV

At the 15th cycle, it was performed a retention test for 2500 s at 500 mV. Figure 3.16 shows the retention results at LRS and HRS after SET and RESET the device respectively. The device maintained very stable in both states, with a current of 19.4 µA at the low resistivity state (LRS) and 0.38 µA at the high resistivity state (HRS). The current ratio between the two states is around 50, which is sufficient to distinguish the two resistivity states. Nonetheless, as seen in figure 3.17, the device has lost the capacity to have two distant states at reading voltage (after hit the compliance it went abruptly to the HRS) leading to failure.

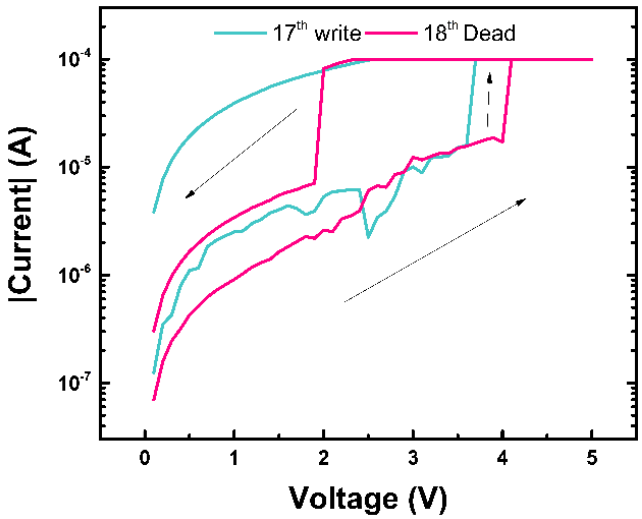

Figure 3.17 - SET process in 17th and 18th cycle, evidencing the device failure

3.5.3 Two printing steps of 40% ZnO:5% EC with silver top contact (40ZnO2Ag)

Compared to the previous substrate, the only change was the use of silver contacts instead of carbon contacts. In this case the positive bias was connected to the platinum and the silver contact was grounded. In figure 3.18, resuming the endurance tests performed, all I-V sweeps performed used a delay time of 200 ms, a current compliance of 1 mA for the SET process, a voltage step of 100 mV. In this case the first IV sweep made was from 0 to 7 V, indicating that the device was in LRS. Therefore, it was executed a positive sweep with the purpose to reset the device. At 16 V the current started to drop from 200 mA to 10 µA. However, when the voltage was decreasing to zero, the device became unstable where the current increase and decrease abruptly. That occurrence happened in all RESET process. On the other side, the set process was more stable, where the SET voltage increased from -4.4 V at 1st cycle to -12.8 at 3rd cycle.

Making the reading test at 500 mV for 100s shows the resistance in HRS varies from 14 MΩ at 2nd cycle to 110 MΩ at 3rd cycle and the LRS varies from 69 kΩ at 1st cycle to 875 kΩ at 3rd cycle. Thus the minimum R_{HRS}/R_{LRS} ratio is 16 at the 2nd cycle, which is similar compared to the carbon top electrode devices. Nevertheless, the performance achieved using screen-printed silver top contacts were worse compared using carbon contacts. The SET and RESET take place at higher voltage and it only achieved three cycles instead twenty cycles achieved when using carbon contacts.

When using silver contacts and the same active electrode (platinum as positive) the SET occurs at negative voltages and the RESET happens at positive voltage, which is the opposite compared using carbon electrodes. Also above 8 V, the device starts to be instable with abrupt current changes. It could be explained due to the fact the Ag is not inert and when applying enough potential it oxidises, creating silver whiskers in the active layer [47]. Thus, the instability could be related due to the presence of two opposite mechanisms: oxygen vacancies dominated due to the presence of ZnO and formation of silver whiskers. When these two mechanisms become dominant, it enters in competition, originating spikes and instability. Due to this possibility a new set of samples was fabricated without silver top electrode.

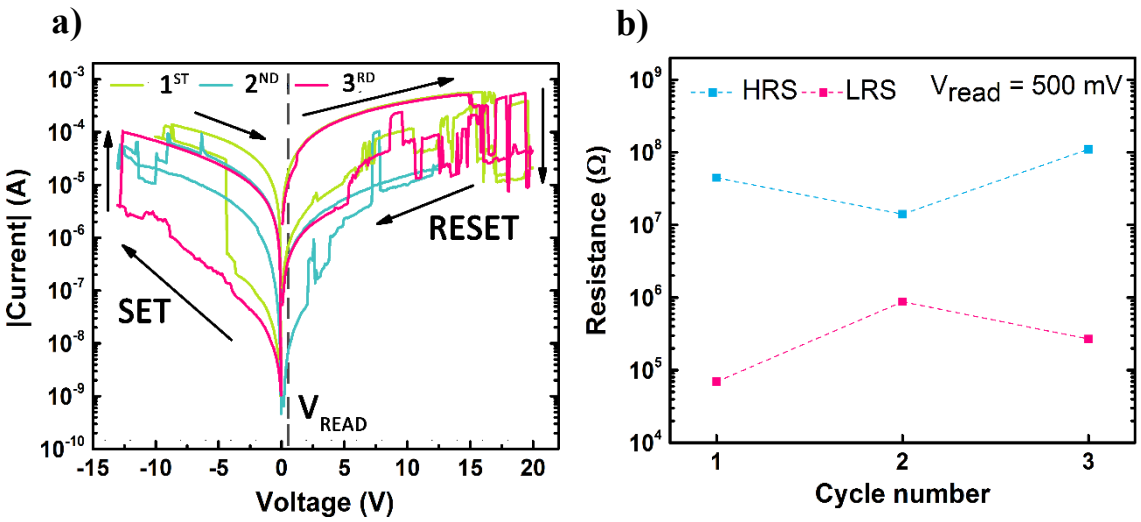

Figure 3.18 - a) Endurance cycles performed on 40 % Zno : 5 % EC with silver top contact and platinum bottom contact on paper substrate **b)** retention tests for 10 s at 500 mV after the SET and RESET the device in a)

3.6 Three printing steps of 40% ZnO:5% EC with carbon top contact (40ZnO3)

In this section it will be discussed the best device performance in terms of cycle endurance, retention time and it will show the unipolar behaviour. Figure 3.19 shows a figure taken by a Leica IC80 HD microscope, using a magnification of 7.5 of the best performance substrate in terms of cycle endurance and also retention time. Making a visual inspection the screen-printed layers are very acceptable due to high opacity across the substrate of the active layer and the carbon electrodes with exception at the top right corner due to mesh obstruction. Also it is apparent the carbon ink slightly spreads which is not relevant due to high electrode area. As depicted in figure 3.19, there are seven different sizes from the smallest with 0.5 mm to the biggest with 2 mm with addictions of 0.25 mm. For each size it has seven contacts making a total of forty-nine devices.

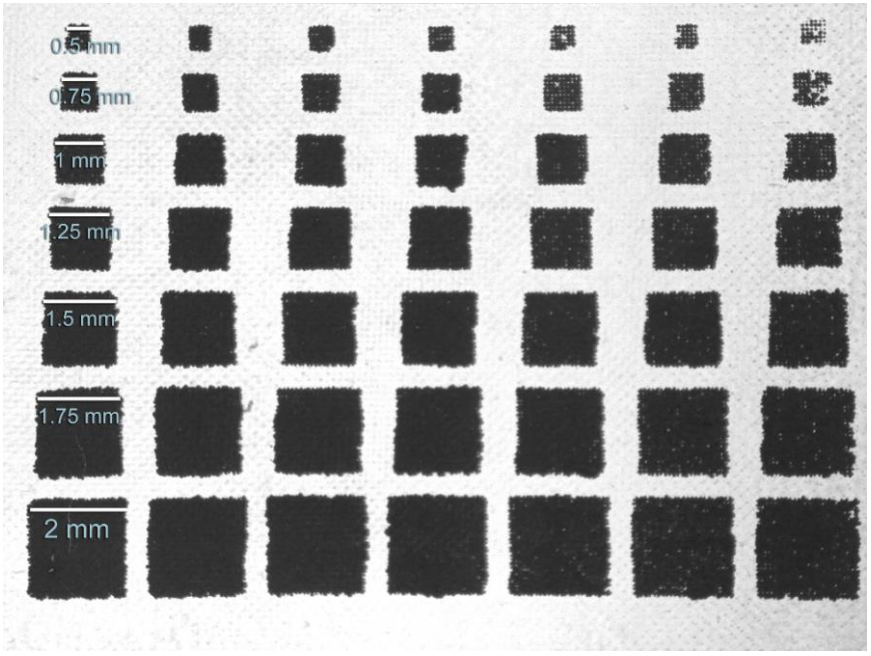

Figure 3.19 - Image of the surface of three printing steps of screen-printed 40% ZnO:5% EC between screen-printed carbon top contacts and E-beam platinum bottom contact on paper substrates

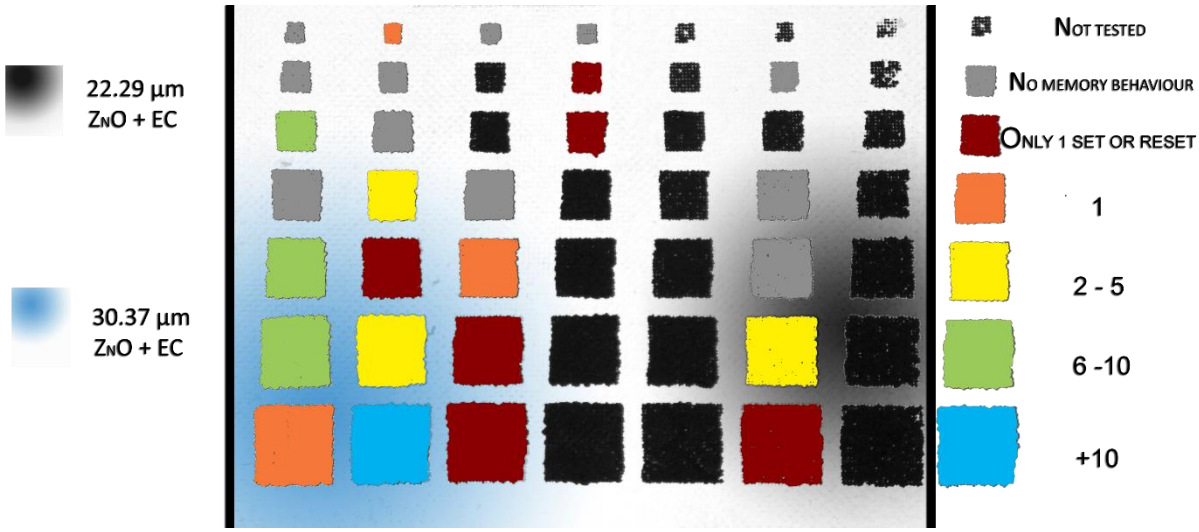

Figure 3.20 - Number of cycles achieved on each contact and also the estimated ZnO:EC layer thickness location in 3.12 c) in blue and 3.12 d) in black

Figure 3.20. shows the number of cycles achieved on each contact and also the estimated active layer thickness location in 3.12 c) and 3.12 d). For three printing steps with higher thickness (shown in blue) have shown better performance where the four devices that achieved six or more cycles, three is near than the contact used to make a cross section image.

3.6.1 Endurance cycles

The best device is identified with the blue colour, that achieved twenty full cycles. The electrical characterization, all I-V sweeps performed used a delay time of 500 ms during SET and 200 ms during RESET process, a current compliance of 0.1 mA only for SET the device, a voltage step of 100 mV and the retention test were performed for 10 s, while applying 500 mV to the platinum contact. Also from the 10th cycle it was stressed running 200 times the following program: perform a positive sweep to 20 V in order to set the device, make a read test for 10 s, at 500 mV, perform a negative sweep to -12 V in order to RESET the device and make a read test for 10 s, at 500 mV.

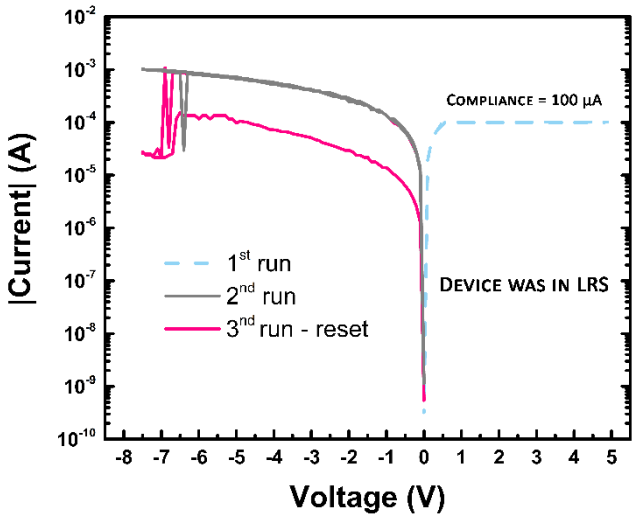

Figure 3.21 - Inicial IV sweep performed in this device

Figure 3.21 shows the initial I-V sweep, from 0 V to 5 V. The level of current reach the compliance of 0.1 mA, meaning the device was in LRS when fabricated. So the next step consists to perform I-V sweeps at negative voltages in order to RESET the device. At the second attempt the device switch from LRS to HRS at -7 V.

In figure 3.22 a), shows the I-V sweeps in which occurred resistive switch. To make the graphic comprehensible, only the first, the tenth and the last cycle are representing by coloured liner. The device was programed to be bipolar where, the SET always occurred at positive voltages and the RESET always happened at negative voltages.

As depicted in figure 3.22 b), the switching probability of the SET and RESET over the voltage is calculated using the data obtained by the I-V sweeps made. The V_{set} and V_{reset} did not occur in a small voltage interval: the V_{set} varies from 3.6 V to 18 V and the V_{reset} varies from -2.2 V to -9.9 V. As in 40ZnO2C, the voltage that occurred the RESET does not follow any tendency (increasing or decreasing) over the cycles. Also, the SET does not follow any tendency over the first cycles.

Annex B complements the data used to create the graphic in 3.22 b), showing the switching voltage for each cycle and the attempt made (the number of trials in order to write or erase the device). Analysing the graphics in figure 3.22 and annex E, is evident the deterioration of the set process over the cycles made. On 17th cycle there were made twenty attempts to successfully write. Another evidence comes from the 16th cycle, with exception at 19th cycle, the write process has occurred when the voltage was decreasing to zero, showing it need more time (or higher electric field) to write due to the use of thick layers (around 30 µm) and the use of Ethyl cellulose as binder in the active layer. By the positive side, compared to the set process, the reset process was very stable and occurred for lower voltages, also the reset process needed at maximum two attempts to achieve the OFF state.

a)

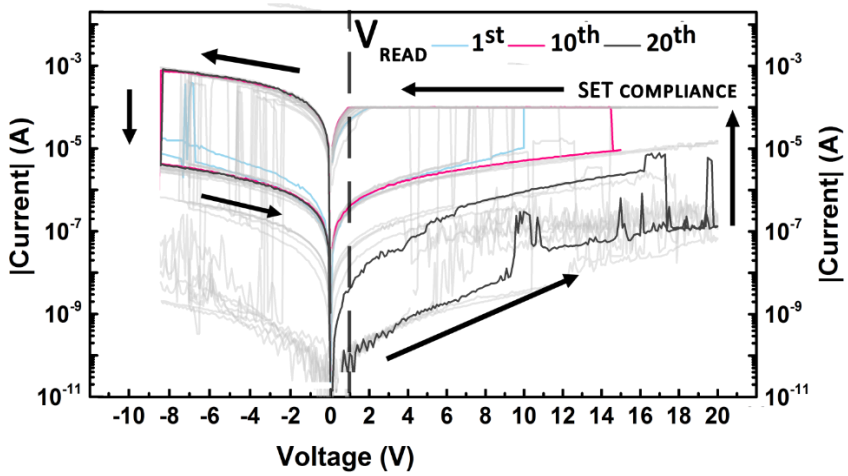

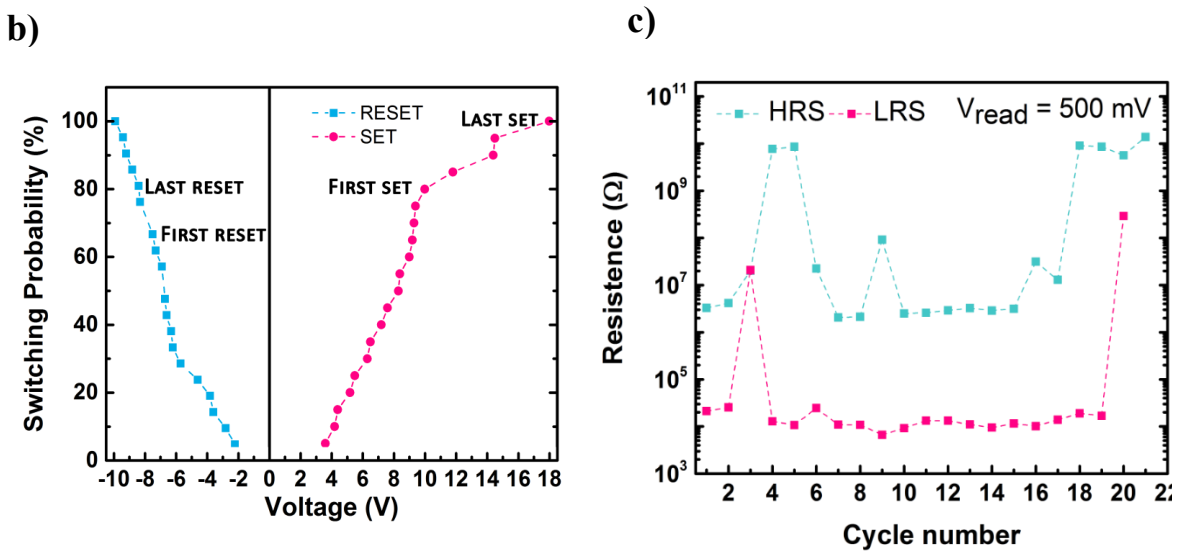

Figure 3.22 - a) Endurance cycles performed on 40 % Zno : 5 % EC with carbon top contact and platinum bottom contact on paper substrate; **b)** Switching probability over voltage **c)** average level of resistence at HSR and LSR after the SET and RESET the device in a)

The most important, despite making high negative voltage sweep (-11 V) and, at 18th cycle the reset occurred at -2.2 V, the device did not set in higher voltage or even enter in disruption, showing a sign of the device stability.

Analysing the reading tests, it is evident at the 3rd set the device remained in OFF state, despite the I-V curve in figure 3.22 a) appeared to successfully SET the device. Moreover, in LRS the resistance value around 10^4 Ω and in the HRS the resistance varies from values around 10^6 Ω and10^{10} Ω. Thus this memory acts as multi-level memory having two different OFF states: one level around 10^6 Ω and another level around 10^{10} Ω. Nevertheless, this is not controllable yet because in table 6.2 in annex E there is not a relation between the V_{reset} and the value of resistance in HRS. Another important aspect is the difference among the LRS and HRS in order to distinguish these two states. With exception for 3th cycle, the difference is more than 1 order of magnitude.

3.6.2 Retention time

In this subsection it will be discussed the maximum retention time achieved in this work. Like for the other devices tested, all I-V sweeps performed used a delay time of 500 ms during set and 200 ms during reset process, a current compliance of 0.1 mA only for the SET process, a voltage step of 100 mV. In annex C and D reveals the performance of this device, which achieved eight cycles. More important, in this device it was made the highest retention test in this work. At 2nd cycle, it was tested at 500 mV for 10 000 s after set and correspondingly after reset the device.

Figure 3.23 shows the device stability performed. In 10 000 s the R_{ON}/R_{OFF} ratio was at least above 1000 which is more than sufficient to distinguish the two states. Also the ON current (LRS) kept stable and the OFF current (HRS) decreased one order of magnitude between 100 and 1000 s. The noise present in the low current state is related to a range problem from the device. Thus this device remained stable during 10 000 s, and after these tests six cycles were made. However, in order to know the retention time of these memories fabricated more tests such as current evolution, which consists make several read at different voltages and find the time when the R_{ON}/R_{OFF} is lower than 10 (when it is lower than 10 the two states cannot be distinguished).

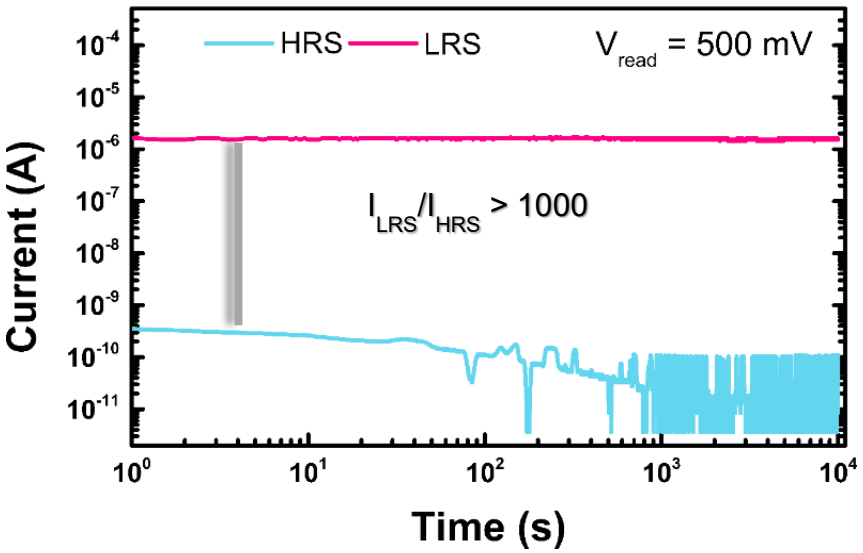

Figure 3.23 - Retention test for 10 000 s at 500 mV after SET and RESET the device

3.7 Study of the switching mechanism mode

As seen above all the devices characterized have shown a bipolar switching mode. It means the RESET occurs at inversed voltage polarity compared to the SET process. However, in 10ZnO, 40ZnO2C, 40ZnO3C and 40ZnO3noUV substrates (figures 3.10, 3.15 and 3.22) some SET switches occurred for higher voltage than the electroforming process. Also the current that occur the RESET is higher than the compliance used in SET. As consequence, these memories do not behave as conventional bipolar. Thus it was programed a setup to test a device to unipolar switching. The device was characterized by applying positive bias to the platinum electrode and the carbon contact grounded. The parameters such as delay time, voltage step, reading voltage and retention time were the same as used previously (500 ms, 100 mV, 500 mV, 10 s).

Figure 3.24 a) represents the unipolar switching of a device tested using the best condition: three printing steps of 40 % Zno : 5 % EC as active layer between carbon top contact and platinum bottom contact (40ZnO3C). After made the first IV sweep, the device was in OFF state. Therefore, it was performed a SET to switch to low resistance state. To achieve unipolar behaviour, the SET process (step 1 to 3) must have a compliance current, which in this case was 100 µA. After successfully switch the device to a low resistive state (LRS), it was performed another positive sweep without compliance to RESET the device (steps 4 and 5). The RESET switch must occur at lower voltage and at higher current. Therefore, at 6.1 V with a current of 0.95 mA the device switched to a HRS. In figure 3.24 b) depicts the retention test of this device that it has an R_{ON}/R_{OFF} ratio around 10^5. However, it will need further investigation in order to correctly determine switching mechanism mode. In this work, it was achieved both mechanisms. Also Fu-Chien Chiu reported unipolar behaviour in resistance switching memory devices using transparent boron doped zinc oxide films [32]. In their work it reffers that defects with deeper trap levels (very likely to exist in ZnO nanoparticles and at te grain boundaries) would be introduced during the deposition processes and could be the origin of nonpolar switching in which both unipolar and bipolar switching behaviors can coexist [32].

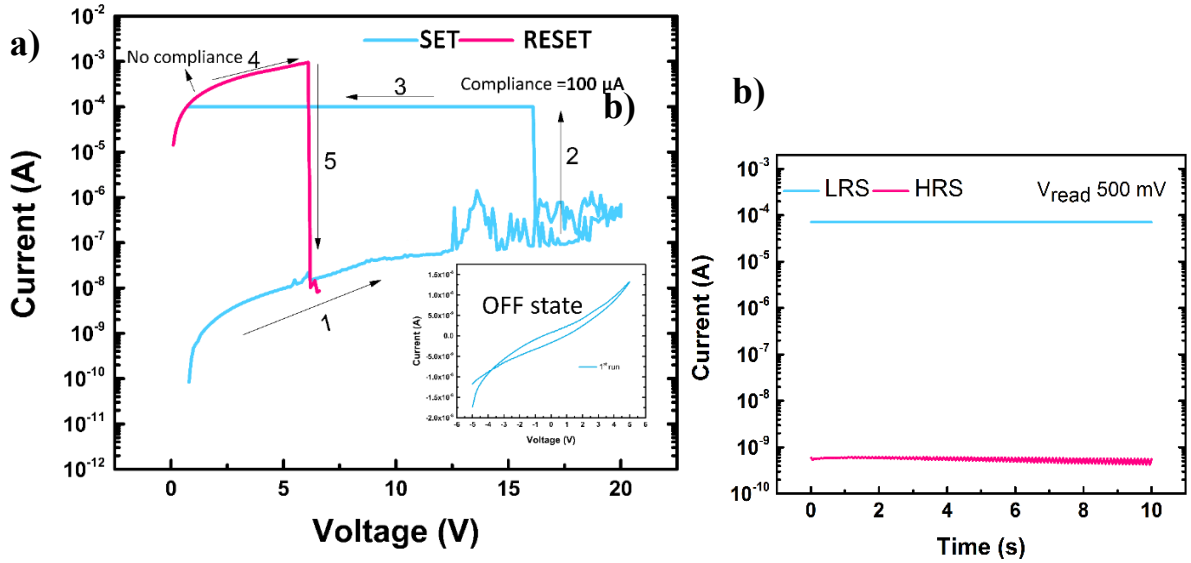

Figure 3.24 – a) Unipolar switching of three printing steps of screen-printed 40% ZnO:5% EC between screen-printed carbon top contacts and E-beam platinum bottom contact on paper substrates **b)** current in LRS and HSR after SET and RESET respectively.

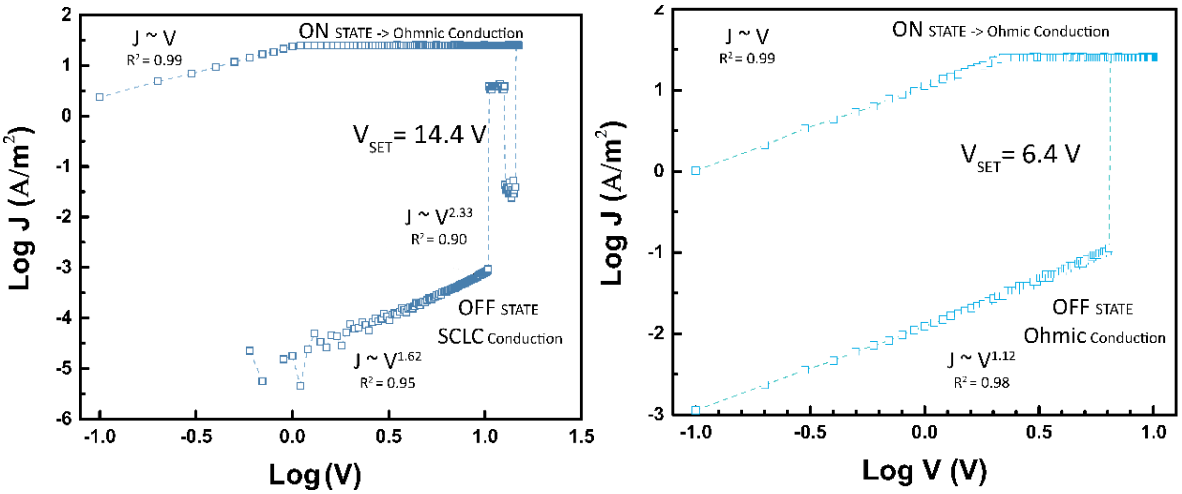

Figure 3.25 - Log J vs log V on a device with a top electrode area of 4 mm^2 on a) 5th SET c) 2nd set

To investigate the carrier transport mechanism of the fabricated devices, the J – V data was fitted in log/log scale, with an appropriate conduction model as is shown in figure 3.25. The data was taken from the SET process in 2nd and 5th cycle of the device characterized in figure 3.25. In figure 3.25 a) the SET takes at high voltages (14.4 V) and in figure 3.25b) the set occurred at lower voltage (6.4 V).

When the SET takes at higher voltages, for the off state (HRS), the data can be well fitted by the space-charge-limited current (SCLC) conduction described below in equation 1:

$$J = \frac{9}{8}\varepsilon_i \mu \frac{V^2}{d^3} \qquad \text{(Eq.1)}$$

Where ε_i is the absolute permittivity of the film, μ the mobility of charge carriers and d is the film thickness. As V is the only term that is not constant, this equation can be rearranged on a logarithmic scale in terms of the voltage dependence to become equation 2:

$$\log(J) = \alpha \log(V) \qquad \text{(Eq.2)}$$

The ideal slope is 2 in order to have a quadratic dependency over current density as described in equation 1. However, in the off state in figure 3.26, two distinct slope regions can be found. The first region the slope is 1.62 with a coefficient of determination of 0.95, meaning the density of current depends on the $V^{1.62}$, which corresponds to Child's Law. In higher voltages, before the switching, the slope increased to 2.33 with a coefficient of determination of 0.90, which it a near trap limit voltage. SCLC conduction has been observed in wide range of materials and it is commonly accepted that the defect-related traps, e.g., oxygen vacancies or deep traps, are contributing to the SCLC conduction [48]. Then the switching could occurs, when the traps in the EC:ZnO layer were filled and the current is suddenly increased to the ON state

On the other side when the switch occurs at low voltage (i.e. in figure 3.11 b)) the Ohmic conduction is the dominant mechanism which the slope is 1.12.

In the ON state, in both cases, the slope is 1.00 which it means the current density linearly depends by voltage, which it means the predominant mechanism in the ON state is Ohmic conduction. Thus the Ohmic conduction can be expressed as in equation 3

$$J = \sigma E = q\mu n \frac{V}{d} \; ; n = N_C \exp\left[-\frac{E_C - E_F}{kT}\right] \qquad \text{(eq. 3.)}$$

Where σ is the electrical conductivity, E is the electrical field between two electrodes, q the number of electrons, N_C is the effective density of states and $E_C - E_F$ is the activation energy. Similarly, as the temperature kept constant during the measurements, V is the only variable, the equation can be rearranged in logarithmic scale:

$$\log(J) = \alpha \log(V) \qquad \text{(Eq.2)}$$

As the current density linearly depends by voltage the slope should be a value close to 1, which it happens in the ON state.

The SCLC mechanism present in HRS combined with the Ohmic conduction present in LRS can support the filament formation [48]. Also a filament model can also explain each of the unipolar and bipolar resistance change by the formation and rupture of the conduction filaments [7] and the presence of multi current states by the number of filaments remained after RESET the device.

According to the filament model, when the film is in the LRS, the current is transported through the conductive filaments, so Ohmic conduction is observed. At RESET voltage, however, most of the filaments are thermally ruptured by Joule heating and the films switch from the LRS to the HRS. In the HRS, at low applied voltages the current is transported through the remained filaments, so Ohmic conduction is also observed. At high voltages, however, SCLC conduction dominates the current transport.

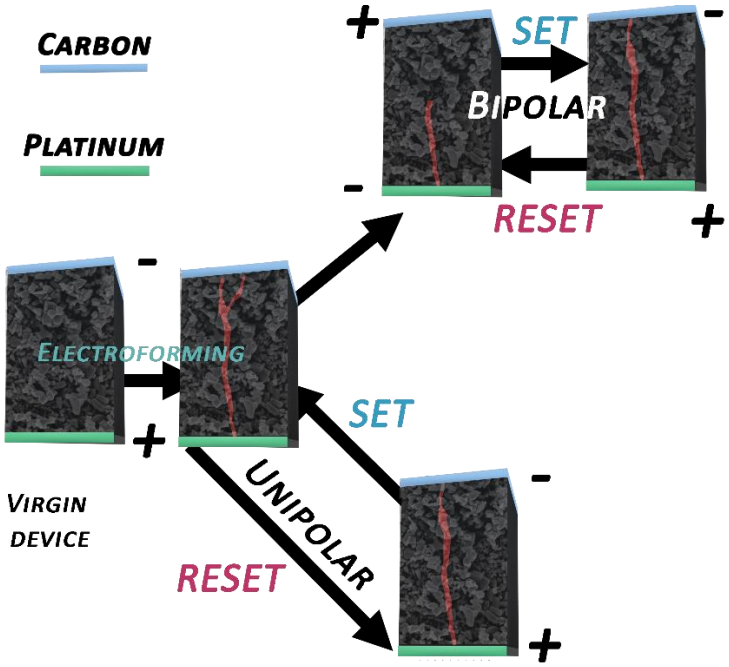

Figure 3.26 – Explanation of the filament mechanis in bipolar and unipolar resistance change

The schematic in figure 3.26, tries to explain the filament mechanism in bipolar and unipolar resistance change. When, making the first I-V sweep and the current is very low, it means the deceive is virgin and a conductive filament is not formed. Electroforming consists the creation of the conductive filament and a larger voltage is needed. In unipolar behaviour the RESET is considered soft, since the complete filament is not destroyed (i.e. if the device has several filaments, the unipolar switch consists to brake one filament). By the other hand, bipolar behaviour the RESET is considered hard (hard RESET) since the filament is broken.

Nevertheless, to discover the filament composition is crucial to perform electrical measurements with variation of temperature. So in this case it will need to perform several cycles and respective current reading to a range of temperatures. The variation of the value of HRS and LRS over the temperature can confirm if hopping mechanism is present and could be a conductive filament of ZnO or a EC conductive filament since neither Carbon or Platinum existing at the electrodes form a conductive filament [28, 44].

4 CONCLUSIONS AND FUTURE PERSPECTIVES

In this present work, the main objectives were successfully achieved:

ZnO RRAM were fabricated on paper substrate, which two of three layers that constitute the device were made using printing techniques, namely screen-printing. With quantity variation of the semiconductor (ZnO) and the binder (EC) it were possible to improve the electrical performance and also to find the conduction mechanism.

The electrical characterization of the final devices after finding the best ink and the optimal thickness of the ZnO:EC layer was performed in order to understand its mechanism and to perform cycles endurance. The next two sections are focused to provide some final inferences about the work carried out, as well as some future perspectives.

4.1 Final conclusions

In this work all the layers that constitutes the device, with exception the bottom electrode, were fabricated using screen-printing technique. Even it was used a manual homemade screen-printing technique this technique was proven to be very useful since several devices worked as RRAM.in visual inspections made, it revealed lack of uniformity through the substrate in special when printing the ZnO:EC layer, which it was confirmed with cross sections images, as in this work the annealing temperature was relatively low at 120 °C, it was possible to create ZnO:EC RRAM on paper substrates. The major advantages of using paper as substrate are related to low cost and biodegradability. These two characteristics permitted to create cheap and "green" RRAM devices since screen-printing technique is also a low cost deposition technique and the inks used in this work are not harmful to the environment.

Fundamentally the active layer constitution and its thickness are crucial to the device behaviour as a RRAM. With these facts the ink formulation was studied as well the number of printing steps. Thus, using three printing steps of an ink containing the highest concentration of ZnO NPs (40% wt) embedded in EC between evaporated platinum bottom contact and screen-printed carbon top contact (40ZnO3C), it has achieved the best performance. In that substrate the best device achieved 20 cycles which the V_{set} varied from 3.6 V to 18 V and the V_{reset} varied from -2.2 V to -9.9 V. These values could be justified by having very thick active layer above 10 µm, positively this difference between the two resistivity states is higher than 10 in the worst situation. Also this device proved to have 2 levels of resistance when the device is an OFF state. However, this is not programmable yet since it was not found a relation between the OFF resistance and the V_{reset}. In other device in the same substrate was able to achieve a retention time of 2 hours and 47 minutes which it is a good indicator of stability. However, the delay time used was 500 ms which it could mean this memory might have a slow response and could be incompatible to high speed applications.

When studding the switching mechanism mode, both mechanisms (unipolar and bipolar) were achieved in different devices. However, the instable bipolar resistive switching is due to growth of filaments during cycles. The required voltages for on/off states fluctuate in the range of ~ 5 V which is a strong evidence of non-consistent bipolar resistive switching.

The switching behaviours are associated with the electron trapping mechanism by the ZnO NPs. For the off state, the data can be well fitted by SCLC, were the density of current depends on the $V^{1.62}$, which corresponds to Child's Law. In higher voltages, before the switching, the relation is $J = V^{2.33}$, which it is a near trap limit voltage. In the ON state the mechanism present is Ohmic conduction.

The SCLC mechanism present at higher voltages in HRS combined with the Ohmic conduction present in both states can support the filament formation.

UV irradiation after printing the active layer have achieved better performance due to the elimination of solvents in the substrate that could cause electrical failure and the creation of Zn^{2+} radicals that induce more carries. However, with this work it cannot identify the nature of the filament and also

the exact role of EC in the resistive memory switching. Thus further work should be carried in order to explain the role of EC and the cause of filament formation.

4.2 Future perspectives

Regarding the RRAM has several publications [7, 20-27, 29, 32, 49] and its reported working principle is beginning to be understood, only a few have used printing process or used on paper substrate [28]. The present work is a novelty since by using paper substrate and using screen-printing technique to deposit 2 of the 3 layers that constitutes the device it was possible to develop a ZnO RRAM. Nevertheless, it will need more optimization in order to improve the electrical performance and yield fabrication. In the next paragraphs are written some aspects that should be considered in future works.

The use of an automatic screen-printing station will greatly improve device yield, because the lack of uniformity seen in manual screen printing is eliminated. So studding the snap-off, shear rate, angle, geometry and squeegee type could be investigated in order to achieve the optimal thickness of the ZnO:EC layer.

Additionally, the incorporation of ZnO nanostructures synthetized by sonochemical method, replacing the commercial ZnO NPs used in inks, could be beneficial promoting better electrical conduction, improving the performance.

Fully printed is another future improvement, since the platinum bottom electrode is deposited using E beam evaporation technique, which is expensive. One solution is to replace the platinum by screen-printed carbon, which makes the device have symmetric electrodes. Also it is important to study if symmetric contacts would lead to any change in electrical performance.

Make a study, in order to understand if exists a dependence between the electrode area and the device performance. Also to check if the EC has a crucial role and its degradation through UV irradiation, it is important to make a study where several substrates was fabricated and the only difference was the irradiation time after deposit the active layer.

The observations for conducting paths were most frequently reported in conductive atomic force microscopy (CAFM) characterizations[49]. Though a powerful tool is CAFM, the microscopic nature of the filaments such as the composition as well as the chemical state are not easy to be clarified by this method.

In terms of electrical characterization, a lot of measurements should be done to fully understand his mechanism. To confirm the SCLC mechanism or another mechanism to confirm the type of filament it is crucial to perform electrical measurements with variation of temperature. Also it will need to perform a pulse switch (ac switch) to test his response (switching speed) and endurance since the pulse switch causes less thermal stress and the device could achieve more cycles. Finally, it will need to make longer retention measurements.

5 BIBLIOGRAPHY

1. Jung, Y.H., et al., *High-performance green flexible electronics based on biodegradable cellulose nanofibril paper.* Nat Commun, 2015. **6**.
2. Widmer, R., et al., *Global perspectives on e-waste.* Environmental Impact Assessment Review, 2005. **25**(5): p. 436-458.
3. Robinson, B.H., *E-waste: An assessment of global production and environmental impacts.* Science of The Total Environment, 2009. **408**(2): p. 183-191.
4. Needhidasan, S., M. Samuel, and R. Chidambaram, *Electronic waste – an emerging threat to the environment of urban India.* Journal of Environmental Health Science and Engineering, 2014. **12**: p. 36-36.
5. Irimia-Vladu, M., *"Green" electronics: biodegradable and biocompatible materials and devices for sustainable future.* Chemical Society Reviews, 2014. **43**(2): p. 588-610.
6. Azam, K., et al., *Study of transport properties of copper/zinc-oxide-nanorods-based Schottky diode fabricated on textile fabric.* Semiconductor Science and Technology, 2013. **28**(12): p. 125006.
7. Lee, S., et al., *Resistive switching characteristics of ZnO thin film grown on stainless steel for flexible nonvolatile memory devices.* Applied Physics Letters, 2009. **95**(26): p. 262113.
8. Hoffman, R.L., B.J. Norris, and J.F. Wager, *ZnO-based transparent thin-film transistors.* Applied Physics Letters, 2003. **82**(5): p. 733-735.
9. Carcia, P.F., et al., *Transparent ZnO thin-film transistor fabricated by rf magnetron sputtering.* Applied Physics Letters, 2003. **82**(7): p. 1117-1119.
10. Hong, K., et al., *Printed, sub-2V ZnO Electrolyte Gated Transistors and Inverters on Plastic.* Advanced Materials, 2013. **25**(25): p. 3413-3418.
11. Gaspar, D., et al., *Nanocrystalline cellulose applied simultaneously as the gate dielectric and?the substrate in flexible field effect transistors.* Nanotechnology, 2014. **25**(9): p. 094008.
12. Iguchi, M., S. Yamanaka, and A. Budhiono, *Bacterial cellulose—a masterpiece of nature's arts.* Journal of Materials Science, 2000. **35**(2): p. 261-270.
13. Lizundia, E., et al., *Increased functional properties and thermal stability of flexible cellulose nanocrystal/ZnO films.* Carbohydrate Polymers, 2016. **136**: p. 250-258.
14. Kubacka, A., M. Fernández-García, and G. Colón, *Advanced Nanoarchitectures for Solar Photocatalytic Applications.* Chemical Reviews, 2012. **112**(3): p. 1555-1614.
15. Liu, A., et al., *Clay Nanopaper with Tough Cellulose Nanofiber Matrix for Fire Retardancy and Gas Barrier Functions.* Biomacromolecules, 2011. **12**(3): p. 633-641.
16. Sehaqui, H., et al., *Fast Preparation Procedure for Large, Flat Cellulose and Cellulose/Inorganic Nanopaper Structures.* Biomacromolecules, 2010. **11**(9): p. 2195-2198.
17. Lindström, S.B., et al., *Mechanosorptive creep in nanocellulose materials.* Cellulose, 2012. **19**(3): p. 809-819.
18. Mohanta, K., S.K. Batabyal, and A.J. Pal, *pn-Junction Rectifiers Based on p-ZnO and n-ZnO Nanoparticles.* Chemistry of Materials, 2007. **19**(15): p. 3662-3666.
19. Lee, M.J., et al., *Two Series Oxide Resistors Applicable to High Speed and High Density Nonvolatile Memory.* Advanced Materials, 2007. **19**(22): p. 3919-3923.
20. Waser, R., et al., *Redox-Based Resistive Switching Memories – Nanoionic Mechanisms, Prospects, and Challenges.* Advanced Materials, 2009. **21**(25-26): p. 2632-2663.

21. Sawa, A., *Resistive switching in transition metal oxides.* Materials Today, 2008. **11**(6): p. 28-36.
22. Szot, K., et al., *Switching the electrical resistance of individual dislocations in single-crystalline SrTiO3.* Nat Mater, 2006. **5**(4): p. 312-320.
23. Waser, R., *Nanotechnology Volume 3: Information Technology I*, ed. 3. 2008, Weinheim: Wiley-VCH.
24. Huang, Y., et al., *Unipolar resistive switching of ZnO-single-wire memristors.* Nanoscale Research Letters, 2014. **9**(1): p. 381-381.
25. Peng, C.-N., et al., *Resistive switching of Au/ZnO/Au resistive memory: an in situ observation of conductive bridge formation.* Nanoscale Research Letters, 2012. **7**(1): p. 559-559.
26. Younis, A., D. Chu, and S. Li, *Bi-stable resistive switching characteristics in Ti-doped ZnO thin films.* Nanoscale Research Letters, 2013. **8**(1): p. 154-154.
27. Chiang, Y.D., et al., *Single-ZnO-Nanowire Memory.* IEEE Transactions on Electron Devices, 2011. **58**(6): p. 1735-1740.
28. Lien, D.-H., et al., *All-Printed Paper Memory.* ACS Nano, 2014. **8**(8): p. 7613-7619.
29. Xu, H., et al., *Effect of Co doping on unipolar resistance switching in Pt/Co:ZnO/Pt structures.* Journal of Alloys and Compounds, 2016. **658**: p. 806-812.
30. Chiu, F.-C., P.-W. Li, and W.-Y. Chang, *Reliability characteristics and conduction mechanisms in resistive switching memory devices using ZnO thin films.* Nanoscale Research Letters, 2012. **7**(1): p. 1-9.
31. Onlaor, K., T. Thiwawong, and B. Tunhoo, *Bi-stable switching behaviors of ITO/EVA:ZnO NPs/ITO transparent memory devices fabricated using a thermal roll lamination technique.* Organic Electronics, 2016. **31**: p. 19-24.
32. Chiu, F.-C., *Conduction Mechanisms in Resistance Switching Memory Devices Using Transparent Boron Doped Zinc Oxide Films.* Materials, 2014. **7**(11): p. 7339.
33. Jaber, B. and L. Laânab, *One step synthesis of ZnO nanoparticles in free organic medium: Structural and optical characterizations.* Materials Science in Semiconductor Processing, 2014. **27**: p. 446-451.
34. Youngil, L., et al., *Large-scale synthesis of copper nanoparticles by chemically controlled reduction for applications of inkjet-printed electronics.* Nanotechnology, 2008. **19**(41): p. 415604.
35. Atkinson, J.K., et al., *An investigation of the performance characteristics and operational lifetimes of multi-element thick film sensor arrays used in the determination of water quality parameters.* Sensors and Actuators B: Chemical, 1999. **54**(3): p. 215-231.
36. Cranny, A., et al., *Sensors for Corrosion Detection: Measurement of Copper Ions in 3.5% Sodium Chloride Using Screen-Printed Platinum Electrodes.* IEEE Sensors Journal, 2012. **12**(6): p. 2091-2099.
37. Cao, X., et al., *Screen Printing as a Scalable and Low-Cost Approach for Rigid and Flexible Thin-Film Transistors Using Separated Carbon Nanotubes.* ACS Nano, 2014. **8**(12): p. 12769-12776.
38. Shaheen, S.E., et al., *Fabrication of bulk heterojunction plastic solar cells by screen printing.* Applied Physics Letters, 2001. **79**(18): p. 2996-2998.
39. Horwood, R.J., *Towards a Better Understanding of Screen Print Thickness Control.* ElectroComponent Science and Technology, 1974. **1**(2): p. 129-136.
40. Wojcik, P.J., *Printable organic and inorganic materials for flexible electrochemical devices*. 2013, Faculdade de Ciências e Tecnologia Universidade Nova de Lisboa.

41. Inukai, K., et al., *Rheological analysis of ceramic pastes with ethyl cellulose for screen-printing.* Ceramics International, 2015. **41**(4): p. 5959-5966.
42. Marani, D., et al., *Influence of hydroxyl content of binders on rheological properties of cerium–gadolinium oxide (CGO) screen printing inks.* Journal of the European Ceramic Society, 2015. **35**(5): p. 1495-1504.
43. Fekete, M., et al., *Photoelectrochemical water oxidation by screen printed ZnO nanoparticle films: effect of pH on catalytic activity and stability.* Nanoscale, 2014. **6**(13): p. 7585-7593.
44. Kreupl, F.B., Rainer; Majewski, Petra; Philipp, Jan B.; Symanczyk, Ralf; Happ, Thomas; Arndt, Christian; Vogt, Mirko; Zimmermann, Roy; Buerke, Axel; Graham, Andrew P.; Kund, Michael, *Carbon Based Resistive Memory.* Digest of the International Electron Devices Meeting (IEDM) 2008, 2009: p. 4.
45. Desai, J., K. Alexander, and A. Riga, *Characterization of polymeric dispersions of dimenhydrinate in ethyl cellulose for controlled release.* International Journal of Pharmaceutics, 2006. **308**(1–2): p. 115-123.
46. Martorano, L.M., C.J. Stork, and Y.V. Li, *UV irradiation-induced zinc dissociation from commercial zinc oxide sunscreen and its action in human epidermal keratinocytes.* Journal of Cosmetic Dermatology, 2010. **9**(4): p. 276-286.
47. Chudnovsky, B.H. *Degradation of power contacts in industrial atmosphere: silver corrosion and whiskers*. in *Electrical Contacts, 2002. Proceedings of the Forty-Eighth IEEE Holm Conference on*. 2002.
48. Lim, E. and R. Ismail, *Conduction Mechanism of Valence Change Resistive Switching Memory: A Survey.* Electronics, 2015. **4**(3): p. 586.
49. Yang, Y.C., et al., *Fully Room-Temperature-Fabricated Nonvolatile Resistive Memory for Ultrafast and High-Density Memory Application.* Nano Letters, 2009. **9**(4): p. 1636-1643.

6 ANNEX

Annex A

Table 6.2 - VSET and VRESET in ecach cycle performed – 40ZnO2C

CYCLE NUMBER	V_{SET}	V_{RESET}
1	5	-2.8
2	3.5	-2.8
3	6.8	-6.6
4	5.5	-6.3
5	3.6	-9
6	3.8	-7.1
7	3.5	-5
8	3.3	-8.9
9	4.9	-4.9
10	3.3	-6
11	2.5	-7
12	2.8	-7
13	5	-4.3
14	3.6	-2
15	2.5	-4.1
16	3.3	-2
17	3.6	-2.8
18	4	-8

Annex B

Table 6.3 - V_{SET} and V_{RESET} in ecach cycle performed – 40ZnO3C

CYCLE NUMBER	V_{RESET}	RUN ATTEMPT	V_{SET}	RUN ATTEMPT
1	-8.8		10	
2	-7.3		6.3	
3	-6.6		3.6	
4	-6.2		5.5	
5	-6.3		14.4	
6	-6.9		8.4	
7	-6.9		5.2	
8	-3.6		9.2	
9	-6.7		9.4	
10	-8.4		14.5	

11	-8.3	**1**	9.3	**2**
12	-3.8	**3**	7.2	**5**
13	-4.6	**6**	11.8	**6**
14	-9.4	**8**	8.3	**8**
15	-9.9	**10**	9	**12**
16	-5.7	**13**	7.6	**13**
17	-9.2	**14**	6.5	**34**
18	-2.2	**35**	4.2	**38**
19	-2.8	**38**	4.4	**39**
20	-7.5	**39**	18	**70**
21	-8.3	**71**		

Annex C

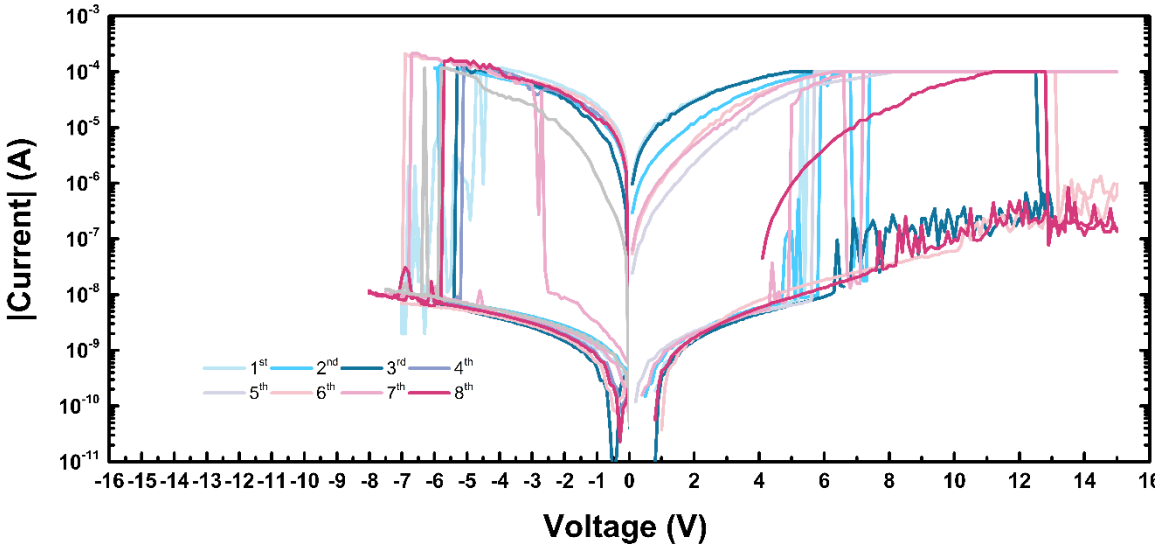

Figure 6.1 - Endurance cycles performed on 40 % Zno : 5 % EC with carbon top contact and platinum bottom contact on paper substrate with UV irradiaton for 15 min

Annex D

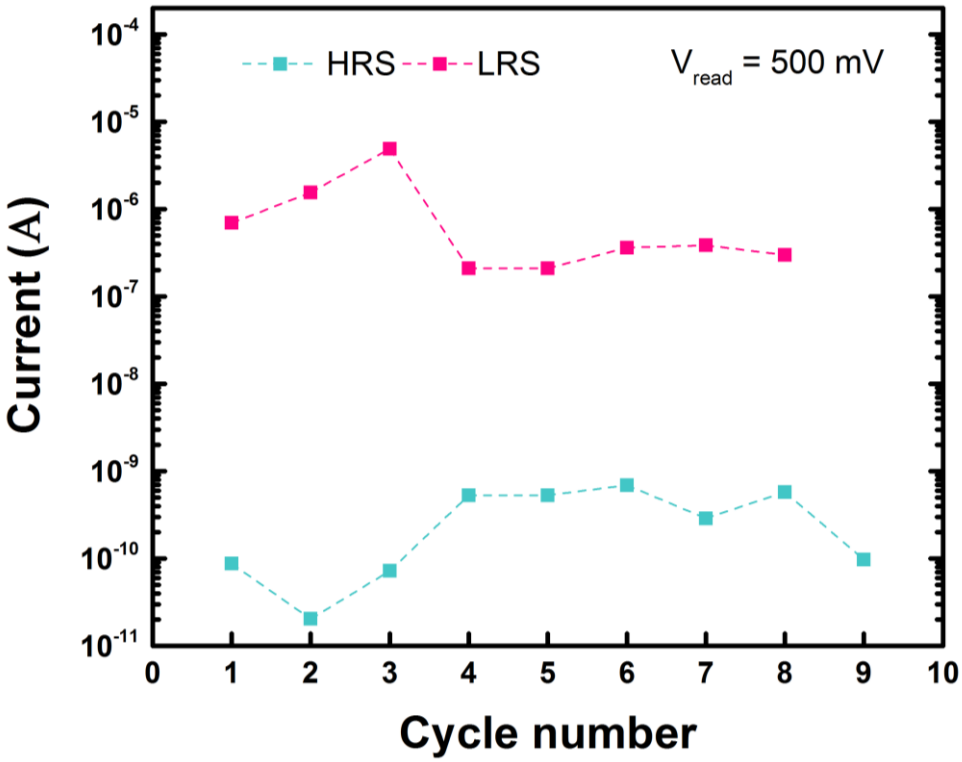

Figure 6.2 - Retention results for 10 s at 500 mV after the SET and RESET the device